ISSN 2732–0189 (Online)
ISSN 1586–2070 (Print)

JOURNAL OF COMPUTATIONAL AND APPLIED MECHANICS

An Open Access International Journal

Published by the University of Miskolc

VOLUME 19, NUMBER 2 (2024)

MISKOLC UNIVERSITY PRESS

ISSN 2732–0189 (Online)
ISSN 1586–2070 (Print)

JOURNAL OF COMPUTATIONAL AND APPLIED MECHANICS

An Open Access International Journal

Published by the University of Miskolc

VOLUME 19 NUMBER 2 (2024)

MISKOLC UNIVERSITY PRESS

Journal of Computational and Applied Mechanics, Vol. 19, No. 2, (2024), pp. 85–104
DOI: 10.32973/jcam.2024.004

THERMOELASTIC ANALYSIS OF FUNCTIONALLY GRADED ANISOTROPIC ROTATING DISKS AND RADIALLY GRADED SPHERICAL PRESSURE VESSELS

Dávid Gönczi
Institute of Applied Mechanics, University of Miskolc
Miskolc-Egyetemváros, H-3515 Miskolc, Hungary
mechgoda@uni-miskolc.hu

[Received: June 10, 2024; Accepted: August 23, 2024]

Abstract. This work deals with the thermoelastic problem of a functionally graded cylindrically anisotropic rotating disk with arbitrary thickness profile subjected to combined axisymmetric thermal and mechanical loads. The material properties are arbitrary functions of the radial coordinate and temperature. A coupled system of ordinary differential equations is derived and the boundary value problem is transformed to an initial value problem, the unknown functions are the stress function and the components of the displacement field. This method uses a state vector formalism to present an effective way to calculate the stress field within monoclinic, orthotropic or isotropic radially graded disks in plane stress state. An analytical solution is presented for the case when the orthotropic material parameters and the thickness profile are specific power-law functions of the radial coordinate and the temperature field is arbitrary. The developed numerical method is applied to simpler steady-state thermoelastic problems of functionally graded spherical pressure vessels, where the material properties are arbitrary functions of the temperature field and of the radial coordinate. The developed methods are compared and results obtained from finite element simulations.

Mathematical Subject Classification: 74S99, 74E05
Keywords: Anisotropic disk, thermomechanical analysis, thermal stresses

1. Introduction

Functionally graded materials (FGM) are advanced materials in which the composition gradually changes, resulting in a corresponding change in the material properties according to the function of the structural component, usually in one direction. The gradient interface between the constituent materials produces a smooth transition from one material to the next, which provides great favourable mechanical behaviour and thermal protection. Due to its excellent material properties, the concept of FGM has become more popular in recent years.

Many studies deal with the mechanics of functionally graded materials from various aspects. Numerous books give solutions to linearly elastic problems for nonhomogeneous bodies such as [1–3]. Several papers presented analytical, semi-analytical and numerical solutions for thermomechanical problems of hollow spheres, cylinders, beams and disks. Noda et. al. [4, 5] studied one-dimensional steady-state thermal stress problems for isotropic functionally graded hollow circular cylinders and spheres using the perturbation method, multilayered approach and Green functions. Chen and Lin [6] carried out an elastic analysis for thick cylinders and spherical pressure vessels made of functionally graded materials when the material parameters vary exponentially along the radial coordinate. Nayak et al. [7] and Bayat et al. [8] developed analytical solutions to obtain the radial, tangential and effective stresses within thick spherical pressure vessels made of FGMs subjected to axisymmetric mechanical and thermal loading. The material properties of the vessel depended on the radial coordinate as a power-law function but the Poisson's ratio had constant value. In a paper by Pen and Li [9] a steady-state thermoelastic problem of isotropic radially graded disks with arbitrary radial non-homogeneity was considered. The numerical solution was reduced to a solution of a Fredholm integral equation. A work by Stampouloglou and Theotokoglou [10] gave the exact solutions for a radially non-homogeneous hollow circular cylinder and disk with exponential and power-law based shear modulus and constant Poisson's ratio. The method used the nonhomogeneous compatibility equations of strain and the equilibrium equations of the thermoelastic problem in order to determine the reduced displacement and stresses in a functionally graded component. Jabbary et al. [11] and [12] dealt with the thermoelastic analysis of a functionally graded rotating thick shell with variable thickness subjected to thermo-mechanical loading by using higher-order shear deformation theory. The mechanical properties, except for the Poisson's ratio, are assumed to vary arbitrarily along the investigated spatial coordinate.

Paper [13] presented the displacement and stress fields in a radially graded hollow circular disk subjected to constant angular acceleration, Poisson's ratio and thermal loading. Here a semi-analytical approach was utilized. Boğa and Yildirim [14] solved these problems with the method of complementary functions and investigated parabolic thickness profiles. For isotropic functionally graded hollow circular disks with arbitrary material properties along the radial direction, Gönczi and Ecsedi [15] presented a numerical method to solve the steady-state thermoelastic problem. Similarly to these papers, there are a number of works dealing with isotropic, radially graded structural components, such as [16–19]. Studies [20, 21] by Zheng et al. determined the displacement and stress fields in a radially graded isotropic and fibre-reinforced rotating disks. The governing equations for displacement and normal stresses are solved using the finite difference method. A work by Eraslan et al. [22] presented analytical solutions of an orthotropic disk with a power-law function based profile. The basic equations are transformed into a standard hypergeometric differential equation by means of a suitable transformation, then an analytical solution is obtained in terms of hypergeometric functions.

A work by Tarn [23] derived exact solutions for the temperature field and thermoelastic stresses for inhomogeneous hollow and solid cylinders when some of the material parameters followed a power law distribution; furthermore, the cylinder was subjected to axial force. Sladek et. al. [24] presented a meshless method based on the local Petrov–Galerkin approach which was developed for the stress analysis of two-dimensional, anisotropic, linearly elastic and viscoelastic solids with continuously varying material properties. The analysed domain was divided into small circular subdomains. In paper [25] the nonlinear steady-state heat conduction equation is solved using an iterative power-series method to obtain the temperature field, then the three-dimensional thermoelasticity equations are solved by a power-series solution procedure to determine the displacements and stresses in anisotropic radially graded hollow cylinders. A method is presented where the cylinder is divided into multiple sub-cylinders and the Taylor series is utilized. Chen et. al. [26] dealt with the axisymmetric problems of transversely isotropic elastic materials based on displacement functions, which were the functions of the thickness coordinate.

In Chang et al. [27] the basic equations of thermoelasticity were formulated into a state equation and a state space formalism for generalized anisotropic thermoelasticity accounting for thermomechanical coupling and thermal relaxation was developed. To obtain the solution for weak thermomechanical coupling the method of perturbation with multiple scales was used and the propagation of plane harmonic thermoelastic waves in an anisotropic medium was studied.

Ceniga [28] dealt with an analytical model of thermal stresses originating during the cooling process of an anisotropic solid continuum with uniaxial or triaxial anisotropy. The investigated continuum consisted of anisotropic spherical particles periodically distributed in an anisotropic infinite matrix. Beom [29] presented a formalism for the general solutions of in-plane thermoelastic fields that satisfy the equilibrium equation. An orthotropy rescaling technique is developed to determine the dependence of thermoelastic fields on the dimensionless orthotropy parameter. The complete thermoelastic fields for the original problem can be evaluated from the solutions of the transformed problem by linear transformation with orthotropy rescaling. Yildirim [30] presents a complementary function method to deal with the thermomechanical problem of orthotropic disks. Allam et. al. [31] presents semi-analytical methods to tackle special material distributions. Papers [32, 33] used discretized domains and a variational approach to tackle the problems of orthotropic disks. Besides disks and spherical bodies, functionally graded beams are often used in various engineering applications; papers such as [34, 35] tackle the mechanical analysis and buckling of such beams.

This paper deals with the steady-state thermoelastic problem of a radially graded anisotropic rotating disk and radially graded pressure vessels subjected to axisymmetric thermal and mechanical loads. As we have seen in the presented literature, the models of the axisymmetric disk and sphere problems contain some kinds of restrictions when it comes to — for example – the functions of the material properties, the thickness of the disk, or neglecting the temperature dependency. Our aim is to formulate a more general approach where all of the material properties are arbitrary functions of the radial coordinate r and temperature T, and a further aim is to present an effective way to calculate the stress field. The considered cylindrically anisotropic disk can be seen in Figure 1, where the material of the disk is a radially graded monoclinic material, while Figure 2 shows a sketch of the isotropic hollow spherical body.

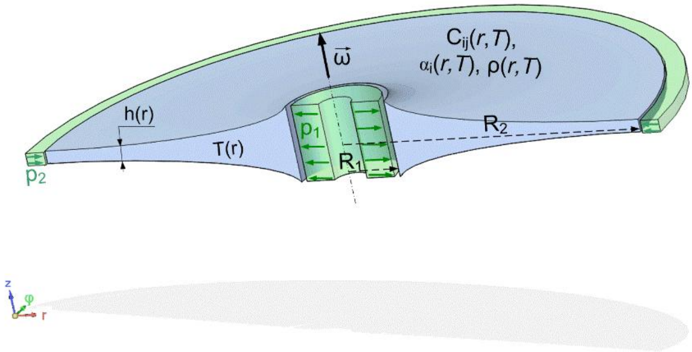

Figure 1. Sketch of a segment of the considered disk with the mechanical and thermal loads

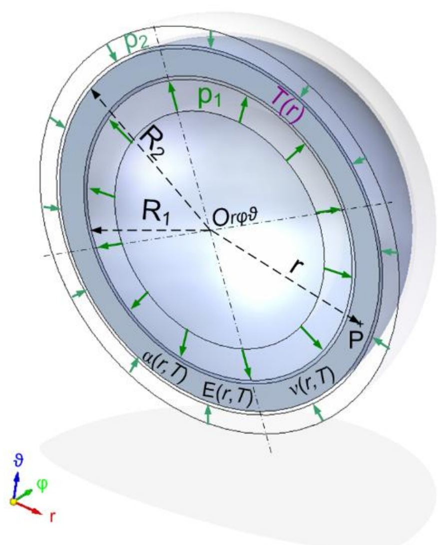

Figure 2. Sketch of a segment of the considered sphere with the mechanical and thermal loads

The thickness of the disk is denoted by $h(r)$, and it is an arbitrary function of the radial coordinate r, where $R_1 \leqslant r \leqslant R_2$, ω is the constant angular velocity. The thermal loading is an arbitrary temperature field $T(r)$ obtained from the solution of the steady-state heat conduction equation. The uniformly distributed mechanical loading exerted on the inner boundary surface is denoted by p_1, while p_2 is the pressure acting on the outer curved boundary surface. For these problems the thermoelastic equations of plane-stress state will be used. A new numerical approach is presented which is based on a coupled system of first-order ordinary differential equations, where the unknown functions are the radial displacement and the stress function.

Anisotropy refers to the directional dependence of material properties. Due to the symmetry, the stiffness tensor $\mathfrak{C}$ contains 21 independent elastic constants.

$$\boldsymbol{\sigma} = \mathbf{C}\boldsymbol{\varepsilon} + \boldsymbol{\beta}T \tag{1a}$$

$$\begin{bmatrix} \sigma_1 \\ \sigma_2 \\ \sigma_3 \\ \tau_{13} \\ \tau_{23} \\ \tau_{12} \end{bmatrix} = \begin{bmatrix} \bar{C}_{11} & \bar{C}_{12} & \bar{C}_{13} & \bar{C}_{14} & \bar{C}_{15} & \bar{C}_{16} \\ & \bar{C}_{22} & \bar{C}_{23} & \bar{C}_{24} & \bar{C}_{25} & \bar{C}_{26} \\ & & \bar{C}_{33} & \bar{C}_{34} & \bar{C}_{35} & \bar{C}_{36} \\ & & & \bar{C}_{44} & \bar{C}_{45} & \bar{C}_{46} \\ & sym. & & & \bar{C}_{55} & \bar{C}_{56} \\ & & & & & \bar{C}_{66} \end{bmatrix} \begin{bmatrix} \varepsilon_1 \\ \varepsilon_2 \\ \varepsilon_3 \\ \gamma_{23} \\ \gamma_{13} \\ \gamma_{12} \end{bmatrix} + \begin{bmatrix} \bar{\beta}_1 \\ \bar{\beta}_2 \\ \bar{\beta}_3 \\ \bar{\beta}_4 \\ \bar{\beta}_5 \\ \bar{\beta}_6 \end{bmatrix} T \tag{1b}$$

where $\boldsymbol{\beta} = -\mathbf{S} \cdot \boldsymbol{\alpha}$, $\mathbf{S}$ is the material compliance tensor, α_i $(i = 1...6)$ are the coefficients of linear thermal expansion, and $\boldsymbol{\sigma}$ and $\boldsymbol{\varepsilon}$ denote the stress strain vectors, respectively. The different types of material anisotropy are determined by the existence of symmetries in the internal structure of the material. This reduces the number of independent stiffness coefficients (monoclinic materials have 13, orthotropic materials have 9, transversely isotropic materials have 5 and isotropic materials have 2 independent parameters) and thermal parameters β_i. In the investigated problems monoclinic materials will be considered. This means that there is one material symmetry plane and for example $C_{i4} = C_{4i} = 0$, $C_{i5} = C_{5i} = 0$, $C_{j6} = C_{6j} = 0$, $(i = 1, 2, 3$ and $j = 4, 5)$

2. Numerical method for disks

We consider a rotating radially graded cylindrically anisotropic disk as shown in Figure 1, and a cylindrical coordinate system $Or\varphi z$ will be used. The strain-displacement relations for disks are [1]:

$$\varepsilon_r(r) = \frac{du(r)}{dr}, \quad \varepsilon_\varphi(r) = \frac{u(r)}{r}, \quad \gamma_{r\varphi}(r) = \frac{dv(r)}{dr} - \frac{v(r)}{r}, \tag{2}$$

where $u = u(r)$ is the radial displacement, $v(r)$ is the tangential displacement, $\gamma_{r\varphi}(r)$ denotes the shear strain and $\varepsilon_r(r)$, $\varepsilon_\varphi(r)$ are the normal strains in the radial and circumferential directions, respectively. In the case of a plane-stress state the stress-strain relationships can be expressed with the following reduced material constants of monoclinic materials:

$$\begin{aligned} &C_{11} = \bar{C}_{11} - \tfrac{\bar{C}_{13}}{\bar{C}_{33}}\bar{C}_{13};\ C_{12} = \bar{C}_{12} - \tfrac{\bar{C}_{23}}{\bar{C}_{33}}\bar{C}_{13};\ C_{16} = \bar{C}_{16} - \tfrac{\bar{C}_{36}}{\bar{C}_{33}}\bar{C}_{13};\ \beta_1 = \bar{\beta}_1 - \tfrac{\bar{\beta}_3}{\bar{C}_{33}}\bar{C}_{13}; \\ &C_{21} = \bar{C}_{21} - \tfrac{\bar{C}_{31}}{\bar{C}_{33}}\bar{C}_{23};\ C_{22} = \bar{C}_{22} - \tfrac{\bar{C}_{23}}{\bar{C}_{33}}\bar{C}_{23};\ C_{26} = \bar{C}_{26} - \tfrac{\bar{C}_{36}}{\bar{C}_{33}}\bar{C}_{23};\ \beta_2 = \bar{\beta}_2 - \tfrac{\bar{\beta}_3}{\bar{C}_{33}}\bar{C}_{23}; \\ &C_{61} = \bar{C}_{61} - \tfrac{\bar{C}_{31}}{\bar{C}_{33}}\bar{C}_{63};\ C_{62} = \bar{C}_{62} - \tfrac{\bar{C}_{32}}{\bar{C}_{33}}\bar{C}_{63};\ C_{66} = \bar{C}_{66} - \tfrac{\bar{C}_{36}}{\bar{C}_{33}}\bar{C}_{63};\ \beta_6 = \bar{\beta}_6 - \tfrac{\bar{\beta}_3}{\bar{C}_{33}}\bar{C}_{63}. \end{aligned} \tag{3}$$

as

$$\sigma_r(r) = C_{11}(T,r)\varepsilon_r(r) + C_{12}(T,r)\varepsilon_\varphi(r) + C_{16}(T,r)\gamma_{r\varphi}(r) + \beta_1(T,r)T(r), \tag{4}$$

$$\sigma_\varphi(r) = C_{21}(T,r)\varepsilon_r(r) + C_{22}(T,r)\varepsilon_\varphi(r) + C_{26}(T,r)\gamma_{r\varphi}(r) + \beta_2(T,r)T(r), \tag{5}$$

$$\tau_{r\varphi}(r) = C_{61}(T,r)\varepsilon_r(r) + C_{62}(T,r)\varepsilon_\varphi(r) + C_{66}(T,r)\gamma_{r\varphi}(r) + \beta_6(T,r)T(r) \tag{6}$$

where σ_r and σ_φ $\tau_{r\varphi}$ are normal stresses, $\tau_{r\varphi}$ is shearing stress, $T(r) = T_a(r) - T_0$ is the temperature difference function, $T_a(r)$ is the absolute temperature, T_0 is the reference temperature, and C_{ij} $(i,j = 1,2,6)$ are stiffness coefficients. The time-independence of the functions involved separates the analysis of the temperature field from that of the elastic field, which means that the problem becomes uncoupled. Therefore the temperature field can be calculated separately from the heat conduction equations, and becomes an input function for this part of the model, which means that $C_{ij}(T(r),r) = C_{ij}(r) = C_{ji}(r)$ and $\beta_i(T(r),r) = \beta_i(r)$. Furthermore, the shearing stress $\tau_{r\varphi}$ is zero due to the axisymmetry, boundary conditions and

$$\frac{\mathrm{d}}{\mathrm{d}r}(rh\tau_{r\varphi}) + h\,\tau_{r\varphi} = 0, \qquad \rightarrow \quad h\tau_{r\varphi} = \frac{F}{r^2}, \rightarrow \quad F = \tau_{r\varphi} = 0. \tag{7}$$

The equilibrium equation in the radial direction has the following form:

$$\frac{\mathrm{d}}{\mathrm{d}r}\left[r\sigma_r(r)h(r)\right] - h(r)\sigma_\varphi(r) + h(r)\rho\omega^2 r^2 = 0\,, \tag{8}$$

where $h(r)$ is the thickness of the disk and ρ denotes the density, which depends on the radial coordinate and the temperature field. The general solution in terms of the stress function $V = V(r)$ is

$$\sigma_r(r) = \frac{1}{r}\frac{V(r)}{h(r)}, \tag{9}$$

$$\sigma_\varphi(r) = \frac{\mathrm{d}V(r)}{\mathrm{d}r}\frac{1}{h(r)} + \rho(r)\omega^2 r^2. \tag{10}$$

After lengthy manipulations of equations (4)-(10) the following system of ordinary differential equations can be derived for the displacement field and the stress function in cylindrically anisotropic radially graded disks:

$$\frac{\mathrm{d}}{\mathrm{d}r}\begin{bmatrix} u \\ V \\ v \end{bmatrix} = \begin{bmatrix} L^f_{11} & L^f_{12} & 0 \\ L^f_{21} & L^f_{22} & 0 \\ L^f_{31} & L^f_{32} & L^f_{33} \end{bmatrix}\begin{bmatrix} u \\ V \\ v \end{bmatrix} + \begin{bmatrix} L^T_{11} \\ L^T_{12} \\ L^T_{13} \end{bmatrix} T + \begin{bmatrix} 0 \\ -\omega^2 h\rho r^2 \\ 0 \end{bmatrix}, \tag{11}$$

$$\frac{\mathrm{d}}{\mathrm{d}r}\mathbf{f} = \mathbf{L}^f\mathbf{f} + \mathbf{L}^T T + \mathbf{L}^\omega, \tag{12}$$

where the following notations were introduced:

$$
\begin{gathered}
L_{01}=\frac{C_{12}C_{66}-C_{16}C_{62}}{C_{11}C_{66}-C_{16}^2},\ L_{11}^f(r)=-L_{01}\frac{1}{r},\ L_{12}^f(r)=\frac{C_{66}}{C_{11}C_{66}-C_{16}^2}\frac{1}{hr},\\
L_{21}^f(r)=\left[C_{22}-C_{21}L_{01}+C_{26}\left(\frac{C_{16}}{C_{66}}L_{01}-\frac{C_{26}}{C_{66}}\right)\right]\frac{h}{r},\ L_{22}^f(r)=L_{01}\frac{1}{r},\\
L_{31}^f(r)=\left(\frac{C_{16}}{C_{66}}L_{01}-\frac{C_{26}}{C_{66}}\right)\frac{1}{r},\ L_{32}^f(r)=\left(\frac{-C_{16}}{C_{11}C_{66}-C_{16}^2}\right)\frac{1}{hr},\ L_{33}^f(r)=\frac{1}{r},\\
L_{11}^T(r)=-\frac{C_{66}\beta_1-C_{16}\beta_6}{C_{11}C_{66}-C_{16}^2},\ L_{13}^T(r)=\frac{-C_{16}L_{11}^T}{C_{66}}-\frac{\beta_6}{C_{66}},\\
L_{12}^T(r)=\left(\beta_2+C_{21}L_{11}^T+C_{26}L_{13}^T\right)h,\\
C_{ij}(r,T(r)),\ \beta_i(r,T(r)),\ \rho(r,T(r));\quad i=1,2,6.
\end{gathered}
\tag{13}
$$

For isotropic radially graded disks the following expressions are used:

$$
\begin{gathered}
L_{11}^f(r)=\frac{-\nu(r,T)}{r},\ L_{12}^f(r)=\frac{1-[\nu(r,T)]^2}{E(r,T)hr},\\
L_{21}^f(r)=E(r,T)\frac{h}{r},\ L_{22}^f(r)=-L_{11}^f(r),\\
L_{31}^f(r)=L_{32}^f(r)=L_{33}^f(r)=L_{13}^T(r)=v(r)=0,\\
L_{11}^T(r)=\alpha(r,T)\left[1+\nu(r,T)\right],\ L_{12}^T(r)=-E(r,T)\alpha(r,T)h,
\end{gathered}
\tag{14}
$$

where $E(r,T(r))=E(r)$ is the Young's modulus, $\alpha(r,T(r))=\alpha(r)$ is the coefficient of linear thermal expansion and $v(r,T(r))=v(r)$ denotes the Poisson ratio. The next phase is the determination of the initial values for the system of differential equations (11). The stress boundary conditions of the rotating disk can be expressed in terms of the stress function as

$$\sigma_r(R_1)=-p_1,\quad \sigma_r(R_2)=-p_2, \tag{15}$$

$$V(R_1)=-p_1R_1h_1,\quad V(R_2)=-p_2R_2h_2, \tag{16}$$

where h_1 and h_2 are the thickness values at the inner and outer cylindrical boundary surfacesQ. Our aim is to formulate an initial value problem for the coupled system of differential equations (11). Two numerical solutions $[u_I(r);V_I(r)]$ and $[u_{II}(r),V_{II}(r)]$ are needed to determine the initial values of the considered two-point boundary value problem. The system of equations is reduced to:

$$\frac{\mathrm{d}}{\mathrm{d}r}u=L_{11}^fu+L_{12}^fV+L_{11}^TT,\quad \frac{\mathrm{d}}{\mathrm{d}r}V=L_{21}^fu+L_{22}^fV+L_{21}^TT-\omega^2h\rho r^2. \tag{17}$$

For the calculations, the fourth-fifth order Runge-Kutta-Fehlberg method will be used in our numerical examples. The input values for the system of differential equations (17) are shown in Table 1. The initial values for the displacements are different arbitrary values, for the stress functions the stress boundary condition — equation (16) – is used.

Table 1. Numerical solution of the thermoelastic problems

Calculations of the initial values		Input values for $u(r)$		Input values for $V(r)$
Calc. I	Eqns. (17)	$u_I(R_1) = u_1$	u_1 (arbitrary)	$V_I(R_1) = -p_1 R_1 h_1$
Calc. II	Eqns. (17)	$u_{II}(R_1) = u_2$	$u_2 \neq u_1$	$V_{II}(R_1) = -p_1 R_1 h_1$
Final Problem	Eqns. (11)	u_3	Calculated with equation (18)	$V_I(R_1) = -p_1 R_1 h_1$

Using the solutions of calculations I and II, the initial value for the displacement field of the original problem can be computed as

$$u(R_1) = u_3 = u_1 + \frac{(u_2 - u_1)\left[-p_2 R_2 h_2 - V_I(R_2)\right]}{V_{II}(R_2) - V_I(R_2)}. \tag{18}$$

The validity of this statement follows from the linearity of the considered thermoelastic boundary value problem. With the displacement field and the stress function, the normal stresses and displacement field can be determined with equation (9) and

$$\sigma_\varphi(r) = \left(L_{21}^f u + L_{22}^f V + L_{21}^T T\right) h^{-1}. \tag{19}$$

3. Numerical method for spherical pressure vessels

A one-dimensional steady-state thermoelastic problem of an isotropic functionally graded spherical hollow body is considered. The spherical pressure vessel is subjected to arbitrary radial coordinate dependent thermal loading $T(r)$ and constant pressures p_1 and p_2 at the curved boundary surfaces, as we can see in Figure 2. The material properties are arbitrary functions of the radial coordinate and temperature. For this spherically symmetric problem a spherical coordinate system $Or\varphi\vartheta$is used. The strain-displacement and stress-strain relations can be expressed as [1]

$$\varepsilon_r(r) = \frac{du(r)}{dr}, \quad \varepsilon_\varphi(r) = \varepsilon_\vartheta(r) = \frac{u(r)}{r}, \tag{20}$$

$$\begin{aligned}\sigma_r(r) = \frac{E(r,T)}{\left[1+\nu(r,T)\right]\left[1-2\nu(r,T)\right]} \big\{ & \left[1-\nu(r,T)\right]\varepsilon_r r) + 2\nu(r,T)\varepsilon_\varphi(r) - \\ & - \alpha(r,T)\left[1+\nu(r,T)\right]T(r)\big\},\end{aligned} \tag{21}$$

$$\begin{aligned}\sigma_\varphi(r) = \sigma_\vartheta(r) = \frac{E(r,T)}{\left[1+\nu(r,T)\right]\left[1-2\nu(r,T)\right]} \big\{ & \nu(r,T)\varepsilon_r(r) + \varepsilon_\varphi(r) - \\ & - \alpha(r,T)\left[1+\nu(r,T)\right]T(r)\big\}.\end{aligned} \tag{22}$$

The equilibrium equation in the radial direction can be written as

$$\frac{\mathrm{d}\sigma_r}{\mathrm{d}r} + \frac{2(\sigma_r - \sigma_\varphi)}{r} = 0, \tag{23}$$

therefore the general solution of equation (23) in terms of stress function $V(r)$ assumes the forms of

$$\sigma_r = \frac{V}{r^2}, \qquad \sigma_\varphi = \frac{1}{2r}\frac{\mathrm{d}V}{\mathrm{d}r}. \tag{24}$$

The system of ordinary differential equations can be expressed as

$$\frac{\mathrm{d}}{\mathrm{d}r}\begin{bmatrix} u \\ V \end{bmatrix} = \begin{bmatrix} -\frac{2\nu}{(1-\nu)}\frac{1}{r} & \frac{(1-2\nu)(1+\nu)}{(1-\nu)E}\frac{1}{r^2} \\ \frac{2E}{1-\nu} & \frac{2\nu}{1-\nu}\frac{1}{r} \end{bmatrix}\begin{bmatrix} u \\ V \end{bmatrix} + \begin{bmatrix} \frac{1+\nu}{1-\nu} \\ \frac{2E}{1-\nu}r \end{bmatrix}\alpha T. \tag{25}$$

We need three initial value calculations to solve this problem, similarly to our previously presented method. The steps of the solution and the input values can be seen in Table 2.

$$u_3 = u_1 + \frac{u_2 - u_1}{V_{II}(R_2) - V_I(R_2)}(-p_2R_2^2 - V_I(R_2)). \tag{26}$$

Table 2. Numerical solution of the thermoelastic problems

Calculations of the initial values		Input values for $u(r)$		Input values for $V(r)$
Calc. I	Eq. (25)	$u_I(R_1) = u_1$	u_1 (arbitrary)	$V_I(R_1) = -p_1R_1^2 = V_1$
Calc. II	Eqns. (25)	$u_{II}(R_1) = u_2$	$u_2 \neq u_1$	$V_{II}(R_1) = -V_1$
Final Problem	Eqns. (25)	u_3	Calculated with equation (26)	$V(R_1) = V_1$

After the third calculation, the radial normal stress can be calculated according to (24) and the tangential normal stress takes the form of

$$\sigma_\varphi = (1-\nu)^{-1}\left[E\frac{u}{r} + \nu\frac{V}{r^2} + E\alpha T\right]. \tag{27}$$

4. Analytical solution for orthotropic disks

An analytical solution will be derived for the case when the material properties of the cylindrically orthotropic, radially graded rotating disk follow the following power-law based distribution:

$$\begin{aligned} \rho(r) &= \rho_0^0\left(\frac{r}{R_1}\right)^m = \rho_0 r^m, \quad \beta_i(r) = \beta_{i0}^0\left(\frac{r}{R_1}\right)^m = \beta_{i0}r^m, \\ C_{ij}(r) &= C_{ij0}^0\left(\frac{r}{R_1}\right)^m = C_{ij0}r^m; \end{aligned} \qquad i,j = 1,2,6. \tag{28}$$

The thickness profile of the disk is described as $h(r) = h_0 r^w$, the temperature-dependency of the material properties is neglected in this case, but thermal loading comes from an arbitrary temperature field $T(r)$. The combination of the basic equations of thermoelasticity results in the following differential equations for the radial displacement field $u(r)$:

$$K_1\frac{\mathrm{d}^2u}{\mathrm{d}r^2} + K_2\frac{\mathrm{d}u}{\mathrm{d}r} + K_3\frac{u}{r^2} + K_4\frac{T}{r} + \beta_{10}\frac{\mathrm{d}T}{\mathrm{d}r} + K_5 r = 0, \tag{29}$$

where we have introduced the constants

$$K_1 = C_{110}, \quad K_2 = C_{110}(m+w+1), \quad K_3 = C_{120}(m+w) - C_{220},$$
$$K_4 = \beta_{10}(m+w+1) - \beta_{20}, \quad K_5 = \rho_0\omega^2. \tag{30}$$

The solution of (29) is

$$u(r) = C_1 r^{g_1} + C_2 r^{g_2} - \frac{r^{g_1}}{g_3}\int I_{T1}(r)\,\mathrm{d}r + \frac{r^{g_2}}{g_3}\int I_{T2}(r)\,\mathrm{d}r, \tag{31}$$

where C_1 and C_2 are integration constants, moreover

$$\begin{aligned} I_{T1}(r) &= K_4 r^{-g_1} T(r) + K_5 r^{g_4} + \beta_{10} r^{g_5} \frac{\mathrm{d}T(r)}{\mathrm{d}r}, \\ I_{T2}(r) &= K_4 r^{-g_2} T(r) + K_5 r^{g_5} + \beta_{10} r^{g_7} \frac{\mathrm{d}T(r)}{\mathrm{d}r}, \end{aligned} \tag{32}$$

$$\begin{aligned} g_{1,2} &= \frac{K_1 - K_2 \pm g_3}{2K_1}, \quad g_3 = \sqrt{(K_2 - K_1)^2 - 4K_3K_1}\,, \\ g_{6,4} &= \frac{3K_1 + K_2 \pm g_3}{2K_1}, \quad g_{7,5} = \frac{K_1 + K_2 \pm g_3}{2K_1}. \end{aligned} \tag{33}$$

Substituting these results into equations (2), (4)-(6) we obtain the functions of the radial normal stress σ_r and tangential normal – or hoop – stress σ_φ:

$$\sigma_r(r) = C_1 S_{r;1}(r) + C_2 S_{r;2}(r) + S_{r;3}(r) + S_{r;4}(r), \tag{34}$$

$$\sigma_\varphi(r) = C_1 S_{\varphi;1}(r) + C_2 S_{\varphi;2}(r) + S_{\varphi;3}(r) + S_{\varphi;4}(r). \tag{35}$$

The following notations are used in equations (34) and (35):

$$\begin{aligned} S_{r;1}(r) &= r^{m+g_1-1}(g_1C_{110} + C_{120}), \\ S_{r;2}(r) &= r^{m+g_2-1}(g_2C_{110} + C_{120}), \\ S_{r;3}(r) &= r^m\Bigg[(g_2C_{110} + C_{120})\frac{r^{g_2-1}}{g_3}\int I_{T2}(r)\,\mathrm{d}r - \\ &\qquad - (g_1C_{110} + C_{120})\frac{r^{g_1-1}}{g_3}\int I_{T1}(r)\,\mathrm{d}r\Bigg], \\ S_{r;4}(r) &= r^m\left[C_{110}\left(\frac{r^{g_2}}{g_3}I_{T2}(r) - \frac{r^{g_1}}{g_3}I_{T1}(r)\right) + \beta_{10}T(r)\right], \end{aligned} \tag{36}$$

and

$$\begin{aligned} S_{\varphi;1}(r) &= r^{m+g_1-1}(g_1C_{120} + C_{220}), \\ S_{\varphi;2}(r) &= r^{m+g_2-1}(g_2C_{120} + C_{220}), \\ S_{\varphi;3}(r) &= r^m\Bigg[(g_2C_{120} + C_{220})\frac{r^{g_2-1}}{g_3}\int I_{T2}(r)\,\mathrm{d}r - \\ &\qquad - (g_1C_{120} + C_{220})\frac{r^{g_1-1}}{g_3}\int I_{T1}(r)\,\mathrm{d}r\Bigg], \\ S_{\varphi;4}(r) &= r^m\left[C_{120}\left(\frac{r^{g_2}}{g_3}I_{T2}(r) - \frac{r^{g_1}}{g_3}I_{T1}(r)\right) + \beta_{20}T(r)\right]. \end{aligned} \tag{37}$$

The constants of integrations can be calculated from the stress boundary conditions (15) as

$$C_1 = \frac{S_{r;2}(R_1)\left[p_2 + S_{r;3}(R_2) + S_{r;4}(R_2)\right] - S_{r;2}(R_2)\left[p_1 + S_{r;3}(R_1) + S_{r;4}(R_1)\right]}{S_{r;2}(R_2)S_{r;1}(R_1) - S_{r;2}(R_1)S_{r;1}(R_2)}, \tag{38}$$

$$C_2 = \frac{S_{r;1}(R_2)\left[p_1 + S_{r;3}(R_1) + S_{r;4}(R_1)\right] - S_{r;1}(R_1)\left[p_2 + S_{r;3}(R_2) + S_{r;4}(R_2)\right]}{S_{r;2}(R_2)S_{r;1}(R_1) - S_{r;2}(R_1)S_{r;1}(R_2)}. \tag{39}$$

In this case the circumferential displacement is zero $v(r) = 0$

Temperature field. For the determination of the temperature field we will consider the case when there are no internal heat sources, the constant temperature values of the cylindrical boundary surfaces t_1 and t_2 are given, moreover there are symmetric, radial coordinate dependent thermal boundary conditions of the third kind on the lower and upper boundary surfaces. This convective heat exchange is given by the temperature of the surrounding medium $t_{env}(r)$ and the heat exchange coefficient $\vartheta(r)$. According to Fourier's law of heat conduction, the heat flow can be expressed as

$$q_r = -\lambda_{11}\frac{\partial T}{\partial r} - \lambda_{12}\frac{1}{r}\frac{\partial T}{\partial \varphi}, \qquad q_\varphi = -\lambda_{12}\frac{\partial T}{\partial r} - \lambda_{22}\frac{1}{r}\frac{\partial T}{\partial \varphi}, \tag{40}$$

where λ_{11}, λ_{12} and λ_{22} are the coefficients of thermal conductance of the anisotropic material. In this axisymmetric case the temperature field $T(r)$ is the function of the radial coordinate. A multilayered approach will be used to determine the temperature field of the radially graded anisotropic disk with radial coordinate-dependent thermal conductivity. The concentric layers or subdomains have constant but different thicknesses and thermal conductivities $\lambda_{11} = \lambda$, the number of the layers is n, for the i-th layer the heat conduction equation takes the forms of [36]:

$$\nabla\left(t\mathbf{q}\right) + hT(r) = 0, \qquad \frac{\mathrm{d}^2 T_i}{\mathrm{d}r^2} + \frac{1}{r}\frac{\mathrm{d}T_i}{\mathrm{d}r} - {p_i}^2\left(T_i(r) - t_{env,\,i}\right) = 0, \tag{41}$$

where we have introduced the notation p_i as

$$R_{mi} = \frac{R_i + R_{i+1}}{2}, \quad \lambda_i = \lambda(R_{mi}), \quad h_i = h(R_{mi}), \quad \vartheta_i = \vartheta(R_{mi}), \;\text{ etc.} \tag{42}$$

The temperature values t_1 and $t_n + 1$ are given at the inner and outer radii of the disk, and the solution of the differential equation is

$$\begin{aligned} T_i(r) = {}& \frac{(t_i - t_{envi})K_0(p_iR_{i+1}) - (t_{i+1} - t_{envi})K_0(p_iR_i)}{K_0(p_iR_{i+1})I_0(p_iR_i) - K_0(p_iR_i)I_0(p_iR_{i+1})} I_0(p_ir) + \\ & + \frac{(-t_i - t_{envi})I_0(p_iR_{i+1}) + (t_{i+1} - t_{envi})I_0(p_iR_i)}{K_0(p_iR_{i+1})I_0(p_iR_i) - K_0(p_iR_i)I_0(p_iR_{i+1})} K_0(p_ir) + t_{env}(r), \end{aligned} \tag{43}$$

where $I_0(x)$ and $K_0(x)$ are the modified Bessel functions of the first and second kind and of order zero. The surface temperatures of the adjacent layers are equal, the heat flow of the i-th layer q_i is constant, therefore we get the following equations for the disk:

$$t_{i+1} = T_i(R_{i+1}) = T_{i+1}(R_{i+1}), \quad h_i q_i(R_{i+1}) = h_{i+1} q_{i+1}(R_{i+1}) \quad i = 1, ..., n-1, \tag{44}$$

$$\begin{aligned} q_i(r) = &-\lambda_i p_i \frac{(t_i - t_{envi})K_0(p_i R_{i+1}) - (t_{i+1} - t_{envi})K_0(p_i R_i)}{K_0(p_i R_{i+1})I_0(p_i R_i) - K_0(p_i R_i)I_0(p_i R_{i+1})} I_1(p_i r) - \\ &- \lambda_i p_i \frac{(-t_i - t_{envi})I_0(p_i R_{i+1}) + (t_{i+1} - t_{envi})I_0(p_i R_i)}{K_0(p_i R_{i+1})I_0(p_i R_i) - K_0(p_i R_i)I_0(p_i R_{i+1})} K_1(p_i r) \\ &i = 1, ..., n-1 \end{aligned} \tag{45}$$

The unknown t_i temperature values can be calculated from (45). When there is no heat exchange on the upper and lower boundary surfaces and the temperature dependency is negligible, then the temperature distribution is:

$$T(r) = t_1 + \frac{t_2 - t_1}{\int\limits_{R_1}^{R_2} \frac{1}{\rho\lambda(\rho)} \mathrm{d}\rho} \int\limits_{R_1}^{r} \frac{1}{\rho\lambda(\rho)} \mathrm{d}\rho. \tag{46}$$

Similarly, when there are no internal heat sources and the temperature dependency of $\lambda(r)$ is negligible, the temperature field within spherical bodies can be expressed as:

$$T(r) = t_1 + \frac{t_2 - t_1}{\int\limits_{R_1}^{R_2} \frac{1}{\rho^2\lambda(\rho)} \mathrm{d}\rho} \int\limits_{R_1}^{r} \frac{1}{\rho^2\lambda(\rho)} \mathrm{d}\rho. \tag{47}$$

5. Numerical examples

There are multiple ways to calculate the effective material properties in temperature-dependent FGMs. For the numerical examples the following parameters will be used to describe the temperature dependency [37, 38]:

$$Ep(T) = P_0(P_{-1}T^{-1} + 1 + P_1 T + P_2 T^2 + P_3 T^3), \tag{48}$$

where E_p denotes a material property, P_i $(i = -1...3)$ are material dependent coefficients of temperature (usually T [K]), furthermore for radially graded two-component disks and spheres the following expressions of effective material properties will be utilized:

$$Ep_f(r,T) = [Ep_1(T) - Ep_2(T)]\,[Z(r)]^m + Ep_2(T),$$
$$Z(r) = \frac{r - R_1}{R_2 - R_1}, \quad \text{or} \quad Z(r) = \frac{r}{R_1}, \tag{49}$$

where m is the volume fraction of the FGM and indices 1 and 2 denote the constituent materials in classic FGMs, steel, and ceramic materials.

Example 1. For the first numerical example, a thick radially graded steel–silicon nitride spherical pressure vessel with the following parameters is considered:

Table 3. Material parameters for the metal-ceramic FGM

Material property (E_p)	Metal (stainless steel)			
	P_{m0}	$P_{m1}(10^{-3})$	$P_{m2}(10^{-7})$	$P_{m3}(10^{-10})$
λ(W/mK)	15.39	−1.264	20.92	−7.223
α(1/k)	$12.33 \cdot 10^6$	0.8086	0.0	0.0
E(Pa)	$2.01 \cdot 10^{10}$	0.3079	−6.534	0.0
$V(-)$	0.3262	−0.1	3.797	0.0
Material property (E_p)	**Ceramic (silicon nitride)**			
	P_{c0}	$P_{c1}(10^{-3})$	$P_{c2}(10^{-7})$	$P_{c3}(10^{-10})$
λ(W/mK)	12.723	−1.032	5.466	−7.876
α(1/k)	$3.873 \cdot 10^6$	0.9095	0.0	0.0
E(Pa)	$3.484 \cdot 10^{10}$	−0.307	2.16	−8.946
$V(-)$	0.24	0.0	0.0	0.0

$$R_1 = 0.5\text{ m}, \;\; R_2 = 0.59\text{ m}, \;\; t_{inner} = 250\text{ K}$$
$$t_{outer} = 20\text{ K}, \;\; p_1 = 200\text{ MPa}, \;\; p_2 = 10\text{ MPa}, \;\; m = \{0.2,\, 1,\, 4\}$$

Three cases are investigated with three different volume fractions m. The temperature field in this case can be approximated as[39]:

$$T(r, m = 0.2) = 1.479 \cdot 10^5 r^2 - 3.27 \cdot 10^5 r + 2.701 \cdot 10^5 - 99427 r^{-1} + 13879.7 r^{-2}\;[K],$$
$$T(r, m = 1) = 94650.7 r^2 - 2.15321 r + 183778 - 70336.8 r^{-1} + 10285.8 r^{-2}\;[K],$$
$$T(r, m = 4) = 58516 r^2 - 1.1778 \cdot 10^5 r + 88658 - 30213.3 r^{-1} + 4069.9 r^{-2}\;[K].$$

The calculations were checked by results obtained by finite element simulations with Abaqus. The 3D model was built from 32 homogeneous layers, and coupled temperature-displacement elements were used. They were in good agreement, although the FE solution oscillated significantly at the inner and outer radii of the sphere, which led to greater error. Figure 3 shows the radial displacements and Figure 4 contains the diagrams of the radial normal stresses (lower half between −200 and 10 MPa) and the tangential normal stresses, illustrated with thicker lines.

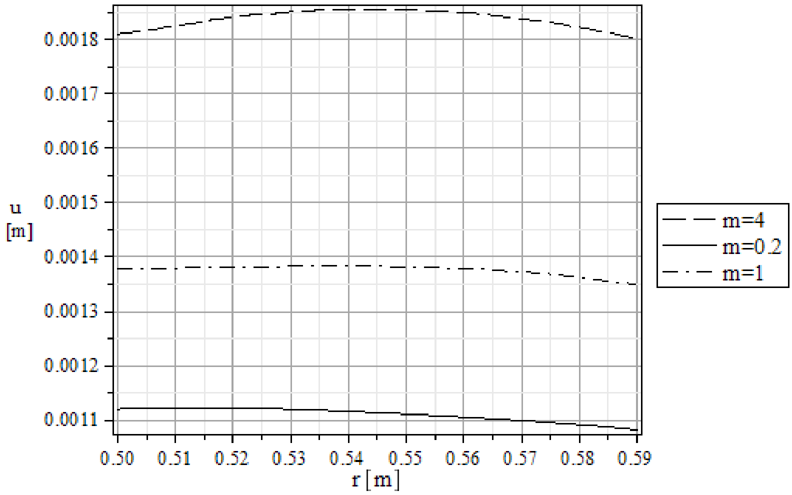

Figure 3. The radial displacements $u(r)$ of the spherical bodies

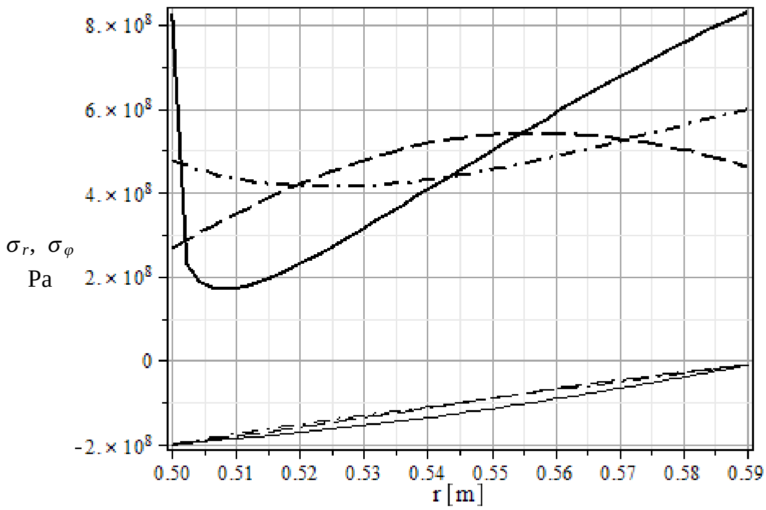

Figure 4. The radial and tangential normal stresses within the spherical pressure vessels

Example 2. In the second numerical example a functionally graded orthotropic disk is considered and the results of the analytical solution and the numerical method are compared to each other. The following numerical data were used:

$$C_{110}^0 = 0.44\,\mathrm{GPa},\ \ C_{120}^0 = 0.32\,\mathrm{GPa},\ \ C_{220}^0 = 16.266\,\mathrm{GPa},$$
$$\rho_0^0 = 4000\frac{\mathrm{kg}}{\mathrm{m}^3},\ \ \beta_{10}^0 = -12476\frac{\mathrm{N}}{\mathrm{m}^2\mathrm{K}},\ \ \beta_{20}^0 = -32500\frac{\mathrm{N}}{\mathrm{m}^2\mathrm{K}},$$
$$a = 0.02\mathrm{m},\ \ b = 0.1\mathrm{m},\ \ h(r) = 10^{-3}r^{-0.2}\,[\mathrm{m}]\,,$$

$$p_1 = 40\text{MPa},\ \ p_2 = 5\text{MPa},\ \ \omega = 100\frac{1}{\text{s}},\ \ t_1 = 120\ \text{K}, t_2 = 20\text{K}$$

$$\lambda(r) = \frac{20}{a^{0.2}} r^{0.2} \left[\frac{\text{W}}{\text{mK}}\right],\ \ \vartheta(r) = \frac{70}{a^{0.2}} r^{0.2} \left[\frac{\text{W}}{\text{m}^2\text{K}}\right],\ \ t_{env}(r) = 95 - 3000 r^{1.8}\ [\text{K}],\ \ n = 12.$$

The results can be seen in Figures 5 and 6. The numerical and analytical results are in good agreement. The average relative error is around 0.01 percent with the Runge-Kutta-Fehlberg method.

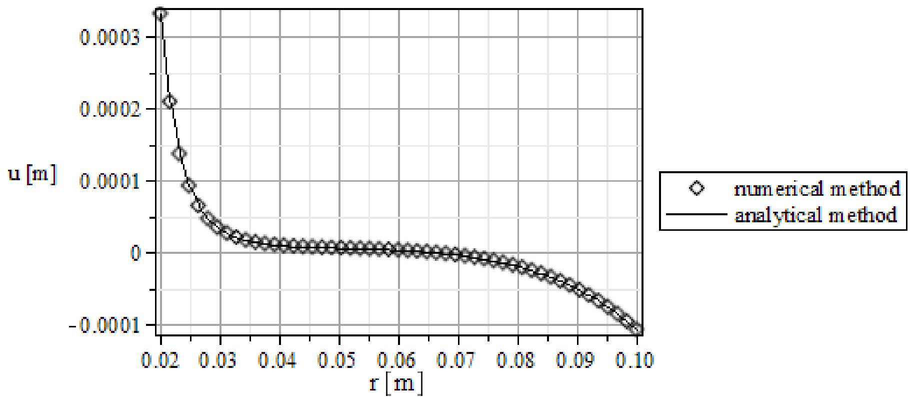

Figure 5. Results of the numerical and analytical methods for the radial displacement fields

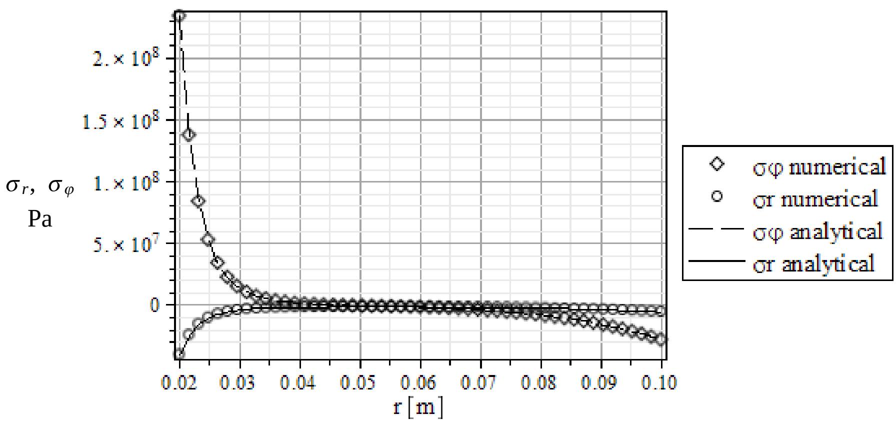

Figure 6. Results of the numerical and analytical methods for the normal stresses

Example 3. For the last example a monoclinic material is considered where the material properties are specific functions of the radial coordinate and the temperature.

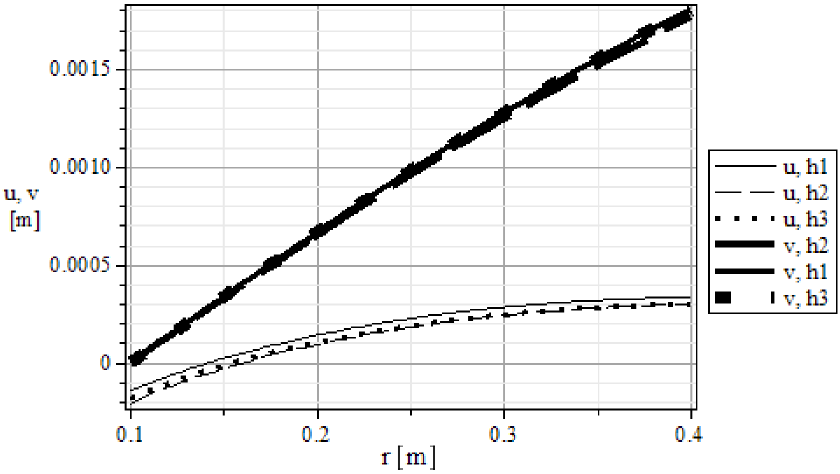

Figure 7. Curves of the radial and tangential displacements

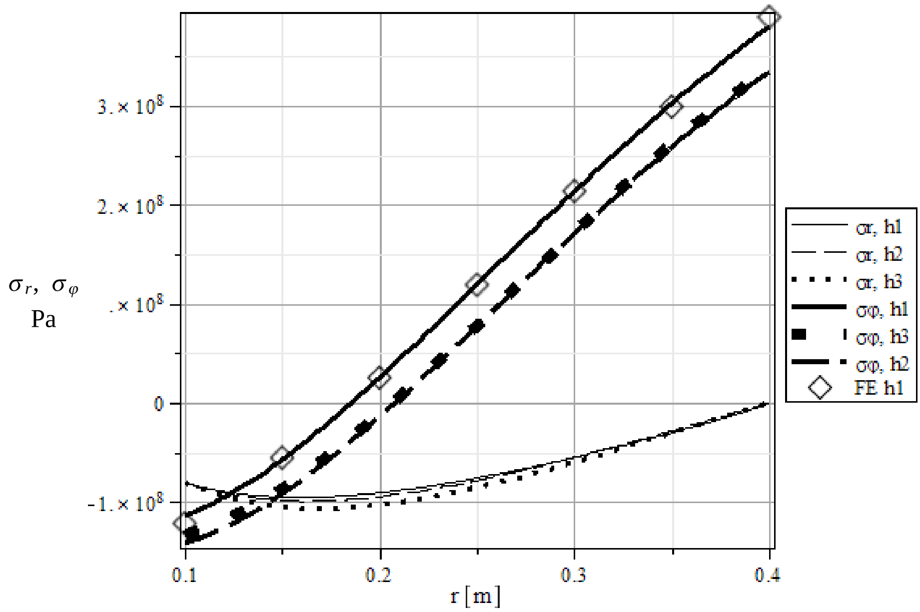

Figure 8. Curves of the radial and tangential normal stresses

The material parameters, geometry and loading are:

$$Z(r,T) = \left(1 + \frac{0.22T}{100}\right)\left(\frac{r}{R_1}\right)^m, \quad C_{11} = 26.43Z(r,T)\,\text{GPa},$$
$$C_{12} = 13,57Z(r,T), \ \text{GPa}, \ C_{22} = 35.7Z(r,T)\,\text{GPa}$$

$$C_{16} = 2.495Z(r,T)\,\mathrm{GPa},\ \ C_{26} = 3.163Z(r,T)\,\mathrm{GPa}$$

$$C_{66} = 8.49Z(r,T)\,\mathrm{GPa},\ \ \rho = 4000Z(r,T)\frac{\mathrm{kg}}{\mathrm{m}^3},$$

$$\beta_1 = -8.03\cdot 10^5 Z(r,T)\frac{\mathrm{N}}{\mathrm{m^2K}},\ \ \beta_2 = -5.234\cdot 10^5 Z(r,T)\frac{\mathrm{N}}{\mathrm{m^2K}},$$

$$\beta_6 = -3.026\cdot 10^5 Z(r,T)\frac{\mathrm{N}}{\mathrm{m^2K}},$$

$$R_1 = 0.1\mathrm{m},\ \ R_2 = 0.4\mathrm{m},\ \ p_1 = 80\mathrm{MPa},\ \ p_2 = 0\mathrm{MPa}$$

$$\omega = 100\frac{1}{\mathrm{s}},\ \ T(r) = -99 - 130\ln(r),\ \ m = 2,$$

$$h_1(r) = -0.266r + 0.01266,\ \ h_2(r) = 0.0115 - 0.0033e^{2r},\ \ h_3(r) = 0.033r^{-0.4}.$$

Three different profiles are investigated with the same volume. The displacement coordinates u, v and the normal stresses are illustrated in Figures 7 and 8. The calculations were checked by results obtained by Abaqus. The disk was modeled with 3D coupled temperature-displacement elements and the body was built from 32 homogeneous temperature-dependent bonded layers. The results are in good agreement, although the tangential normal stresses from the FE method oscillated at the ends of the disk due to the multilayered approach.

With the developed method, the optimal profile for a specific load set can be calculated effectively when used in conjunction with optimization codes.

6. Conclusions

A numerical method was presented to obtain the solution of steady-state thermoelastic problems for radially graded spherical pressure vessels and rotating cylindrically monoclinic disks. A new numerical approach was presented which is based on a coupled system of first-order ordinary differential equations with the displacement and the stress function as unknowns. The original axisymmetric two-point boundary value problem was transformed to an initial value problem based on the basic equations of thermoelasticity and plane-stress state in order to calculate the displacement and stress field. The material properties of spherical bodies and anisotropic disks are arbitrary functions of the radial coordinate and the temperature. The developed methods were checked by an analytical solution of an orthotropic disk where the material distribution follows a power-law function. The results were compared to each other and to results obtained by finite element simulations and they are in good agreement.

References

1. Hetnarski, R. B. and Eslami, M. R. *Thermal Stresses – Advanced Theory and Applications.* Springer, New York, 2010.
2. Lekhnitskii, S. G. *Theory of Elasticity of an Anisotropic Body.* Mir Publishers, Moscow, 1981.
3. Noda, N., Hetnarski, R. B., and Tanigawa, Y. *Thermal Stresses.* Rochester, New York, USA: Lastran Corporation, 2000.

4. Obata, Y. and Noda, N. "Steady thermal stresses in a hollow circular cylinder and a hollow sphere of a functionally gradient materiaL." *Journal of Thermal Stresses,* **17**(4), (1994), 471–487. doi: 10.1080/01495739408946273.
5. Kim, K.S. and Noda, N. "Green's function approach to unsteady thermal stresses in an infinite hollow cylinder of functionally graded material." *Acta Mechanika,* **156**, (2002), pp. 145–161. doi: 10.1007/BF01176753.
6. Chen, Y. Z. and Lin, X. Y. "Elastic analysis for thick cylinders and spherical pressure vessels made of functionally graded materials." *Computational Materials Science,* **44**, (2008), 581–587. doi: 10.1016/j.commatsci.2008.04.018.
7. Nayak, P., Mondal, S. C., and Nandi, A. "Stress, Strain and displacement of a functionally graded thick spherical vessel." *Engineering Science and Technology,* **3**(4), (2011), pp. 2660–2671.
8. Bayat, Y., Ghannad, M., and Torabi, H. "Analytical and numerical analysis for the FGM thick sphere under combined pressure and temperature loading." *Archive of Applied Mechechanics,* **10**, (2011), pp. 229–242. doi: 10.1007/s00419-011-0552-x.
9. Pen, X. and Li, X. "Thermoelastic analysis of functionally graded annulus with arbitrary gradient." *Applied Mathematics and Mechanics (English Edition),* **30**(10), (2010), pp. 1211–1220.
10. Nejad, M. Z. and Theotokoglou, E.E. "The radially nonhomogeneous thermoelastic axisymmetric problem." *International Journal of Mechanical Sciences,* **120**, (2017), pp. 311–321. doi: 10.1016/j.ijmecsci.2016.11.010.
11. Bayat, Y., Jabbari, M., and Ghannad, M. "A general disk form formulation for thermo-elastic analysis of functionally graded thick shells of revolution with arbitrary curvature and variable thickness." *Acta Mechanica,* **228**(1), (2017), pp. 215–231. doi: 10.1007/s00707-016-1709-z.
12. Jabbari, M., Nejad, M.Z., and Ghannad, M. "Thermo-elastic analysis of axially functionally graded rotating thick truncated conical shells with varying thickness." *Composites Part B: Engineering,* **96**, (2016), 20–34. doi: 10.1016/j.compositesb.2016.04.026.
13. Dai, T. and Dai, H. L. "Thermo-elastic analysis of a functionally graded rotating hollow circular disk with variable thickness and angular speed." *Applied Mathematical Modelling,* **40**, (2016), pp. 7689–7707. doi: 10.1016/j.apm.2016.03.025.
14. Boğa, C. and Yildirim, V. "Application of the complementary functions method to an accurate elasticity solution for the radially functionally graded (FG) rotating disks with continuously variable thickness and density." *Solid State Phenomena,* **250**, (2016), pp. 100–105. doi: 10.4028/www.scientific.net/SSP.251.100.
15. Gönczi, D. and Ecsedi, I. "Thermoelastic analysis of functionally graded hollow circular disk." *Archive of Mechanical Engineering,* **62**(1), (2015), pp. 5–18. doi: 10.1515/meceng-2015-0001.
16. Çallioğlu, H., Bektaş, N. B., and Sayer, M. "Stress analysis of functionally graded rotating discs: analytical and numerical solutions." *Archive of Mechanical Engineering,* **27**, (2011), pp. 950–960. doi: 10.1007/s10409-011-0499-8.

17. Jabbari, M., Ghannad, M., and Nejad, M. "Effect of thickness profile and FG function on rotating disks under thermal and mechanical loading." *Journal of Mechanics,* **32**(1), (2016), pp. 35–46. doi: 10.1017/jmech.2015.95.
18. Vandana, G. and Singh, S.B. "Mathematical modeling of creep in a functionally graded rotating disc with varying thickness." *Regenerative Engineering and Translational Medicine,* **2**(3), (2016), pp. 126–140. doi: 10.1007/s40883-016-0018-3.
19. Manish, Garg. "Stress analysis of variable thickness rotating FG disc." *International Journal of Pure and Applied Physics,* **13**(1), (2017), pp. 158–161.
20. Zheng, Y., Bahaloo, H., Mousanezhad, D., Mahdi, E., Vaziri, A., and Nayeb-Mashemi, H. "Stress analysis in functionally graded rotating disks with non-uniform thickness and variable angular velocity." *International Journal of Mechanical Sciences,* **119**, (2017), pp. 283–293. doi: 10.1016/j.ijmecsci.2016.10.018.
21. Zheng, Y., Bahaloo, H., Mousanezhad, D., Mahdi, E., Vaziri, A., and Nayeb-Mashemi, H. "Displacement and stress fields in a functionally graded fiber-reinforced rotating disk with nonuniform thickness and variable angular velocity." *International Journal of Mechanical Sciences,* **139**(3), (2017). doi: 10.1115/1.4036242.
22. Eraslan, A. N., Kaya, Y., and Varli, E. "Analytical solutions to orthotropic variable thickness disk problems." *Pamukkale University Journal of Engineering Sciences,* **22**(1), (2016), pp. 24–30. doi: 10.5505/pajes.2015.91979.
23. Tarn, J. Q. "Exact solutions for functionally graded anisotropic cylinders subjected to thermal and mechanical loads." *International Journal of Solids and Structures,* **38**(46-47), (2016), pp. 8189–8206. doi: 10.1016/S0020-7683(01)00182-2.
24. Sladek, J., Sladek, V., and Zhang, Ch. "Stress analysis in anisotropic functionally graded materials by the MLPG method." *Engineering Analysis with Boundary Elements,* **29**(6), (2005), pp. 597–609. doi: 10.1016/j.enganabound.2005.01.011.
25. Vel, S. S. "Exact thermoelastic analysis of functionally graded anisotropic hollow cylinders with arbitrary material gradation." *Mechanics of Advanced Materials and Structures,* **18**, (2011), pp. 14–31. doi: 10.1080/15376494.2010.519218.
26. Chen, J., Ding, H., and Chen, W. "Three-dimensional analytical solution for a rotating disc of functionally graded materials with transverse isotropy." *Archive of Applied Mechanics,* **77**(4), (2007), pp. 241–251. doi: 10.1007/s00419-006-0098-5.
27. Chang, H. H. and Tarn, J. Q. "A state space formalism and perturbation method for generalized thermoelasticity of anisotropic bodies." *International Journal of Solids and Structures,* **44**, (2007), 956–975. doi: 10.1016/j.ijsolstr.2006.05.034.
28. Ceniga, L. "Thermal stresses in two- and three-component anisotropic materials." *Acta Mechanica Sinica,* **26**, (2010), pp. 695–709. doi: 10.1007/s10409-010-0368-x.

29. Ceniga, L. "Thermoelastic in-plane fields in a linear anisotropic solid." *International Journal of Engineering Science,* **69**, (2013), pp. 43–60. doi: 10.1016/j.ijengsci.2013.03.012.
30. Yildirim, V. "The complementary functions method (CFM) solution to the elastic analysis of polar orthotropic rotating discs." *Journal of Applied and Computational Mechanics,* **4**(3), (2018), pp. 216–230. doi: 10.22055/JACM.2017.23188.1150.
31. Allam, M. N. M., Tantawy, R., and Zenkour, A. M. "Thermoelastic stresses in functionally graded rotating annular disks with variable thickness." *Journal of Theoretical and Applied Mechanics,* **56**(4), (2019), pp. 1029–1041. doi: 10.15632/jtam-pl.56.4.1029.
32. Sondhi, L., Thawait, A. K., Sanyal, S., and Bhowmick, S. "Stress and deformation analysis of variable thickness clamped rotating disk of functionally graded orthotropic material." *Materials Today: Proceedings,* **18**(7), (2019), pp. 4431–4440. doi: 10.1016/j.matpr.2019.07.412.
33. Nayak, P., Bhowmick, P., Saha, K. N., and Bhowmick, S. "Elasto-plastic analysis of thermo-mechanically loaded functionally graded disks by an iterative variational method." *Engineering Science and Technology, an International Journal,* **23**(1), (2019), pp. 42–64. doi: 10.1016/j.jestch.2019.04.007.
34. Kiss, L. P. "Nonlinear stability analysis of FGM shallow arches under an arbitrary concentrated radial force." *International Journal of Mechanics and Materials in Design,* **16**(1), (2020), pp. 901–108. doi: 10.1007/s10999-019-09460-2.
35. Alimoradzadeh M., Saledi, M., and Esfarjani, S. M. "Nonlinear vibration analysis of axially functionally graded microbeams based on nonlinear elastic foundation using modified couple stress theory." *Periodica Polytechnica Mechanical Engineering,* **64**(2), (2020), pp. 97–108. doi: 10.3311/PPme.11684.
36. Carslaw, H. S. and Jaeger, I. C. *Conduction of Heat in Solids.* Clarendon Press, Oxford, 1959.
37. Shen, H. S. *Functionally Graded Materials: Nonlinear Analysis of Plates and Shells.* CRC Press, London, UK, 2009. doi: 10.1201/9781420092578.
38. Touloukian, Y. S., Gerritsen, J. K., and Moore, N. Y. *Thermophysical Properties Research Literature Retrieval Guide.* New York, Plenum Press, 1967.
39. Gönczi, D. "Thermoelastic Problems of Functionally Graded and Composite Structural Components." PhD dissertation. University of Miskolc, 2017.

Journal of Computational and Applied Mechanics, Vol. 19, No. 2, (2024), pp. 105–137
DOI: 10.32973/jcam.2024.005

GREEN FUNCTIONS FOR COUPLED BOUNDARY VALUE PROBLEMS WITH APPLICATIONS TO STEPPED BEAMS MADE OF HETEROGENEOUS MATERIAL

Abderrazek Messaoudi
Institute of Applied Mechanics, University of Miskolc
Miskolc-Egyetemváros, H-3515 Miskolc, Hungary
abderrazek.messaoudi@uni-miskolc.hu

[Received: July 15, 2024; Accepted: December 12, 2024]

Abstract. The main objective of the present paper is to clarify the effect of the axial load on the eigenfrequencies of axially loaded and pinned-pinned stepped beams made of heterogeneous material. To this end, we shall consider how the Green functions of the corresponding coupled boundary value problems can be determined. After finding these Green Functions, the vibration problems of the unloaded and loaded stepped beams are reduced to eigenvalue problems governed by homogeneous Fredholm integral equations. These are solved numerically.

Mathematical Subject Classification: 05C38, 15A15; 05A15, 15A18
Keywords: Green function, stepped beam, vibration, coupled boundary value problem

1. Introduction

Beams can be found in many machines or structures as their vital elements. For that reason their mechanical behavior has been the subject of studies for a long time [1–3].

One of the major topics of interest is their vibrations [4–6]. When it comes to stepped beams, the continuous-mass transfer matrix method is extended in [7] to incorporate further effects such as rotatory inertia. The beams can have multiple steps and can carry an arbitrary number of lumped mass elements. De Rosa et al. [8] consider stepped beams assuming the Euler-Bernoulli hypothesis. The beams rest on an elastic foundation, whose stiffness can change at the steps. The frequency equation is solved numerically. Stepped beams with lumped masses made of axially functionally graded material are investigated in [9] using the lumped mass transfer matrix method. In article [10], the applied method is Adomian Decomposition, which proves to be effective for this kind of issue.

The Green function was first used in 1828 [11] for electrostatic issues. Since then, it has gained ground [12, 13]. Several three-point boundary value issues defined by third-order nonlinear differential equations are discussed in [14] with Green functions. The findings of [15] were extended for degenerated ordinary differential equation systems in [16, 17] for beam vibrations. The topic of stepped beam vibrations with a

Green function technique is addressed in [18], although for fixed-fixed support conditions. Paper [18] is devoted to coupled eigenvalue problems for which it presents a definition of the Green function determined for fixed-fixed stepped beams with the aim of clarifying their vibration problems, including the issue of what happens if the beam is subjected to axial forces.

The paper is organized into six sections. Sections 2 and 3 present the definition of the coupled boundary value problems and the definition of the Green functions that belong to them. The properties of these Green functions are detailed in Section 4. The definition plays an important role in the determination of the Green functions since it is constructive and allows calculation of the Green functions. Section 5 considers what form the coupled eigenvalue problems take. The issue of the stepped beams is tackled in Sections 6 and 7, which together with Section 8 constitute the main part of the present paper. They contain the calculation of the Green functions for the unloaded stepped beams and the axially loaded stepped beams as well. As regards their vibration problems, the corresponding eigenvalue problems are reduced to Fredholm integral equations that are solved numerically. Section 8 presents the numerical solutions for the vibration problem when the beam is axially loaded. The last section contains the concluding remarks.

2. Coupled boundary value problems

We shall consider a pair of inhomogeneous ordinary differential equations (ODEs)

$$L_i[y_i(x)] = r_i(x), \qquad i = 1,2 \tag{1a}$$

where the differential operators $L_i[y_i(x)]$ of order 2κ are defined by the relations

$$L_i[y_i(x)] = \sum_{n=0}^{2\kappa} p_{ni}(x)\, y_i^{(n)}(x), \qquad \frac{\mathrm{d}^n(\ldots)}{\mathrm{d}x^n} = (\ldots)^{(n)}, \qquad i = 1,2. \tag{1b}$$

Note that the order of these ODEs are the same.

Let b be an inner point in the interval $x \in [0, \ell = 1]$ for which it holds that $0 < b < \ell$, $b = \ell_1$, $\ell - b = \ell_2$ and $\ell_1 + \ell_2 = \ell = 1$. It is assumed that $\kappa \geq 1$ is a natural number. The functions ($p_{n1}(x)$ and $r_1(x)$) $\{r_{n2}(x)$ and $r_2(x)\}$ are continuous if ($x \in [0, b)$) $\{x \in (b, \ell = 1]\}$ and $p_{2\kappa i}(x) \neq 0$.

It is assumed that ODEs (1) are associated with the following boundary and continuity conditions:

$$U_{0r}[y_1] = \sum_{n=1}^{2\kappa} \alpha_{nr1}\, y_1^{(n-1)}(0) = 0\,, \qquad r = 1,2,\ldots,\kappa \tag{2a}$$

$$\begin{aligned} U_{br}[y_1, y_2] &= U_{br1}[y_1] - U_{br2}[y_2] = \\ &= \sum_{n=1}^{2\kappa} \Big(\beta_{nr1}\, y_1^{(n-1)}(b) - \beta_{nr2}\, y_2^{(n-1)}(b)\Big) = 0\,, \qquad r = 1,2,\ldots,2\kappa \end{aligned} \tag{2b}$$

$$U_{1r}[y_2] = \sum_{n=1}^{2\kappa} \gamma_{nr2}\, y_2^{(n-1)}(\ell) = 0\,, \qquad r = 1,2,\ldots,\kappa \tag{2c}$$

where α_{nrI}, β_{nrI}, β_{nrII}, and γ_{nrII} are real constants.

ODEs (1) with boundary and continuity conditions (2) determine a coupled boundary value problem, since the solutions $y_1(x)$, $y_2(x)$ should satisfy continuity conditions (2b).

Let us denote the linearly independent particular solutions of ODEs (1b) by $y_{mi}(x)$ $(m = 1, 2, \ldots, 2\kappa)$. With $y_{mi}(x)$, the general solutions $y_i(x)$ are of the form

$$y_1(x) = \sum_{m=1}^{2\kappa} \mathcal{A}_{m1} y_{m1}(x), \qquad \text{if } x \in [0, b]; \tag{3a}$$

$$y_2(x) = \sum_{\ell=1}^{2\kappa} \mathcal{A}_{m2} y_{m2}(x), \qquad \text{if } x \in [b, \ell = 1]; \tag{3b}$$

where $\mathcal{A}_{m1}$ and $\mathcal{A}_{m2}$ are undetermined integration constants.

The integration constants $\mathcal{A}_{\ell 1}$ and $\mathcal{A}_{\ell 2}$ can be obtained from the boundary and continuity conditions:

$$\sum_{m=1}^{2\kappa} \mathcal{A}_{m1} U_{0r}[y_{m1}] = 0, \qquad r = 1, 2, \ldots, \kappa \tag{4a}$$

$$\sum_{m=1}^{2\kappa} \left(\mathcal{A}_{m1} U_{br1}[y_{m1}] - \mathcal{A}_{m2} U_{br2}[y_{m2}] \right) = 0, \qquad r = 1, 2, \ldots, 2\kappa \tag{4b}$$

$$\sum_{\ell=1}^{2\kappa} \mathcal{A}_{m2} U_{1r}[y_{m2}] = 0, \qquad r = 1, 2, \ldots, \kappa\,. \tag{4c}$$

If we know the Green function $G(x, \xi)$ that belongs to the coupled boundary value problem (1), (2), then we seek the solution in the following form:

$$y(x) = \int_{\xi=0}^{\ell=1} G(x, \xi)\, r(\xi)\, \mathrm{d}\xi\,, \tag{5a}$$

where

$$y(x) = \begin{cases} y_1(x) & \text{if } x \in [0, b) \\ y_2(x) & \text{if } x \in (b, \ell = 1] \end{cases} \quad \text{and} \quad r(\xi) = \begin{cases} r_1(\xi) & \text{if } \xi \in [0, b)\,, \\ r_2(\xi) & \text{if } \xi \in (b, \ell = 1]\,. \end{cases} \tag{5b}$$

3. Green's functions of coupled boundary value problems

Let $G(x, \xi)$ be the Green function that belongs to the coupled boundary value problem (1), (2). It is defined by the following formula and properties [18].
Formula:

$$G(x, \xi) = \begin{cases} G_{11}(x, \xi) & \text{if } x, \xi \in [0, b], \\ G_{21}(x, \xi) & \text{if } x \in [b, \ell] \text{ and } \xi \in [0, b], \\ G_{12}(x, \xi) & \text{if } x \in [0, b] \text{ and } \xi \in [b, \ell], \\ G_{22}(x, \xi) & \text{if } x, \xi \in [b, \ell], \end{cases} \tag{6}$$

Properties:

1. Let ξ be an arbitrarily fixed coordinate in $[0, b]$

(i) The function $G_{11}(x, \xi)$ is a continuous function of x and ξ in the triangles $0 \le x \le \xi \le b$ and $0 \le \xi \le x \le b$ – see Figure 1. In addition it is 2κ times differentiable with respect to x and the derivatives

$$\frac{\partial^n G_{11}(x,\xi)}{\partial x^n} = G_{11}^{(n)}(x,\xi)\,, \qquad n = 1, 2, \dots, 2\kappa \tag{7a}$$

are also continuous functions of x and ξ in the triangles $0 \le x \le \xi \le b$ and $0 \le \xi \le x \le b$.

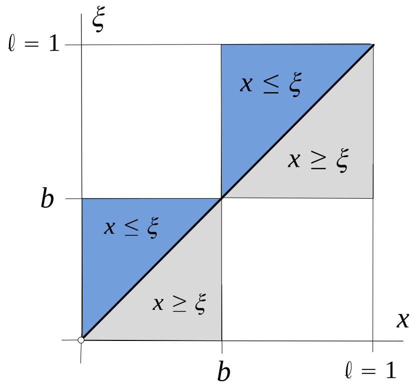

Figure 1. Triangular domains

The function $G_{11}(x, \xi)$ and its derivatives

$$G_{11}^{(n)}(x,\xi) = \frac{\partial^n G_{11}(x,\xi)}{\partial x^n}\,, \qquad n = 1, 2, \dots, 2\kappa - 2 \tag{7b}$$

should be continuous for $x = \xi$:

$$\begin{aligned}
&\lim_{\varepsilon\to 0}\left[G_{11}^{(n)}(\xi+\varepsilon,\xi) - G_{11}^{(n)}(\xi-\varepsilon,\xi)\right] = \\
&\qquad = \left[G_{11}^{(n)}(\xi+0,\xi) - G_{11}^{(n)}(\xi-0,\xi)\right] = 0 \quad n = 0, 1, 2, \dots 2\kappa - 2
\end{aligned} \tag{7c}$$

the derivative $G_{1I}^{(2\kappa-1)}(x, \xi)$ should, however, have a jump if $x = \xi$:

$$\begin{aligned}
&\lim_{\varepsilon\to 0}\left[G_{1I}^{(2\kappa-1)}(\xi+\varepsilon,\xi) - G_{1I}^{(2\kappa-1)}(\xi-\varepsilon,\xi)\right] = \\
&\qquad = \left[G_{1I}^{(2\kappa-1)}(\xi+0,\xi) - G_{1I}^{(2\kappa-1)}(\xi-0,\xi)\right] = \frac{1}{p_{2\kappa 1}(\xi)}.
\end{aligned} \tag{7d}$$

(ii) In contrast, the function $G_{21}(x, \xi)$ and its derivatives

$$G_{21}^{(n)}(x,\xi) = \frac{\partial^n G_{21}(x,\xi)}{\partial x^n}\,, \qquad n = 1, 2, \dots, 2\kappa \tag{7e}$$

are all continuous functions for any x in $[b, \ell]$

2. Let ξ be fixed in $[b,\ell]$.
(i) The function $G_{12}(x,\xi)$ and its derivatives

$$G_{12}^{(n)}(x,\xi)=\frac{\partial^n G_{12}(x,\xi)}{\partial x^n}\,,\qquad n=1,2,\ldots,2\kappa \tag{8a}$$

are all continuous functions for any x in $[0,b]$.
(ii) The function $G_{22}(x,\xi)$ is a continuous function of x and ξ in the triangles $b\le x\le \xi\le\ell$ and $b\le\xi\le x\le\ell$ – see again Figure 1. In addition it is 2κ times differentiable with respect to x and the derivatives

$$\frac{\partial^n G_{22}(x,\xi)}{\partial x^n}=G_{22}^{(n)}(x,\xi)\,,\qquad n=1,2,\ldots,2\kappa \tag{8b}$$

are also continuous functions of x and ξ in the triangles $b\le x\le\xi\le\ell$ and $b\le\xi\le x\le\ell$.

The function $G_{22}(x,\xi)$ and its derivatives

$$G_{22}^{(n)}(x,\xi)=\frac{\partial^n G_{22}(x,\xi)}{\partial x^n}\,,\qquad n=1,2,\ldots,2\kappa-2 \tag{8c}$$

are also continuous for any $x=\xi$ in $[b,\ell]$:

$$\begin{aligned}\lim_{\varepsilon\to 0}&\left[G_{22}^{(n)}(\xi+\varepsilon,\xi)-G_{22}^{(n)}(\xi-\varepsilon,\xi)\right]=\\&=\left[G_{22}^{(n)}(\xi+0,\xi)-G_{22}^{(n)}(\xi-0,\xi)\right]=0\,,\quad n=0,1,2,\ldots 2\kappa-2;\end{aligned} \tag{8d}$$

the derivative $G_{22}^{(2\kappa-1)}(x,\xi)$ should, however, have a jump if $x=\xi$:

$$\begin{aligned}\lim_{\varepsilon\to 0}&\left[G_{22}^{(2\kappa-1)}(\xi+\varepsilon,\xi)-G_{22}^{(2\kappa-1)}(\xi-\varepsilon,\xi)\right]=\\&=\left[G_{22}^{(2\kappa-1)}(\xi+0,\xi)-G_{22}^{(2\kappa-1)}(\xi-0,\xi)\right]=\frac{1}{p_{2\kappa 2}(\xi)}.\end{aligned} \tag{8e}$$

3. Let α be an arbitrary but finite non-zero constant. For a fixed $\xi\in[0,\ell]$ the product $G(x,\xi)\alpha$ as a function of x ($x\ne\xi$) should satisfy the homogeneous differential equations

$$\begin{aligned}L_1\left[G(x,\xi)\alpha\right]=0,\quad &\text{if}\quad x\in[0,b];\\ L_2\left[G(x,\xi)\alpha\right]=0,\quad &\text{if}\quad x\in[b,\ell].\end{aligned} \tag{9}$$

4. The product $G(x,\xi)\alpha$ as a function of x should satisfy the boundary conditions and the continuity conditions

$$\begin{aligned}&\sum_{n=1}^{2\kappa}\alpha_{nr1}\,G^{(n-1)}(0)=0\,, && r=1,\ldots,\kappa\\ &\sum_{n=1}^{2\kappa}\Big(\beta_{nr1}\,G^{(n-1)}(b-0)-\beta_{nr2}\,G^{(n-1)}(b+0)\Big)=0\,, && r=1,\ldots,2\kappa\\ &\sum_{n=1}^{2\kappa}\gamma_{nr2}\,G^{(n-1)}(\ell)=0\,. && r=1,\ldots,\kappa\end{aligned} \tag{10}$$

The above boundary and continuity conditions should be satisfied by the functions pairs

$$\{G_{11}(x,\xi), G_{21}(x,\xi)\}\,,$$
$$\{G_{12}(x,\xi), G_{22}(x,\xi)\}\,,$$

as well.

Remark 1. It can be proved by following the line of thought of a similar proof presented in [17] that the Green function defined above satisfies not only differential equation (1) but boundary and continuity conditions (2) as well.

Remark 2. The definition of the Green function is a constructive one since it makes possible to calculate the elements of the Green function.

Remark 3. Consider the inhomogeneous coupled boundary value problem defined by differential equations (1) with the boundary and continuity conditions (2). Let us assume that we know the corresponding Green function. Then the solution is given by the integral (5).

4. Properties of the Green function

4.1. **Self-Adjointness.** Assume that the functions

$$u(x) = \begin{cases} u_1(x) & \text{if } x \in [0,b] \\ u_2(x) & \text{if } x \in [b,\ell] \end{cases} \tag{11a}$$

and

$$v(x) = \begin{cases} v_1(x) & \text{if } x \in [0,b] \\ v_2(x) & \text{if } x \in [b,\ell] \end{cases}\,. \tag{11b}$$

satisfy the boundary and continuity conditions (2) and are continuously differentiable 2κ times. Then they are called comparison functions. It is obvious that the solutions $y_1(x)$ and $y_2(x)$ of the coupled boundary value problem (1) and (2) are also comparative functions. Formula

$$(u,v)_L = \int_0^b u_1(x)\, L_1[v_1(x)]\,\mathrm{d}x + \int_b^\ell u_2(x)\, L_2[v_2(x)]\,\mathrm{d}x \tag{12}$$

taken on the set of the comparison functions $u(x)$, $v(x)$ is a product defined on the differential operators L_1 and L_2.

The coupled boundary value problem (1) and (2) is said to be self-adjoint if the product (12) is commutative, i.e., it holds that

$$(u,v)_L = (v,u)_L\,. \tag{13}$$

Condition (13) is called the condition of self-adjointness.

It can be proved (see [18]) that the Green function of coupled and self-adjoint boundary value problems is a symmetric function of ξ and x:

$$G(x,\xi) = G(\xi,x)\ . \tag{14}$$

5. Coupled eigenvalue problems

Consider differential equations

$$K_i\,[y_i] = \lambda\, M_i\,[y_i]\,, \qquad i = 1, 2 \tag{15a}$$

where $y_1(x)$, $x \in [0, b]$ and $y_2(x)$, $x \in [b, \ell]$; $(0 < b < \ell = 1)$ are again the unknown functions while λ is an unknown parameter (the eigenvalue sought). Differential operators $K_i\,[y_i]$ and $M_i\,[y_i]$ are defined by the equations

$$\begin{aligned} K_i\,[y_i] &= \sum_{n=0}^{\kappa} (-1)^n \left[f_{ni}(x) y_i^{(n)}(x) \right]^{(n)}\,, \qquad \frac{\mathrm{d}^n(\ldots)}{\mathrm{d}x^n} = (\ldots)^{(n)}\,; \\ M_i\,[y_i] &= \sum_{n=0}^{\mu} (-1)^n \left[g_{ni}(x) y_i^{(n)}(x) \right]^{(n)}\,, \qquad \kappa > \mu \geq 1 \end{aligned} \tag{15b}$$

in which the real function $(f_{ni}(x))$ $[g_{ni}(x)]$ is assumed to be differentiable continuously (κ) $[\mu]$ times and

$$f_{\kappa i}(x) \neq 0 \qquad \text{if } x \in [0, b] \tag{15c}$$

$$g_{\mu i}(x) \neq 0 \qquad \text{if } x \in [b, \ell]\,. \tag{15d}$$

The order of the differential operator on the left side of (15a) – this is 2κ – is greater than 2μ: the latter is the order of the differential operator on the right side.

We shall assume that ODEs (15) are associated with the homogeneous boundary and continuity conditions given by equations (2).

Let $u(x)$ and $v(x)$ $x \in [0, \ell]$ be two comparative functions for the eigenvalue problem (15), (2) – see (11). If we perform successive partial integration we get the following formulae for the products $(u, v)_K$ and $(u, v)_M$:

$$\begin{aligned} (u, v)_K = {} & \left[\sum_{n=0}^{\kappa} \sum_{r=0}^{n-1} (-1)^{(n+r)} u_1^{(r)}(x) \left[f_{n1}(x)\, v_1^{(n)}(x) \right]^{(n-1-r)} \right]_0^{b-0} + \\ & + \left[\sum_{n=0}^{\kappa} \sum_{r=0}^{n-1} (-1)^{(n+r)} u_2^{(r)}(x) \left[f_{n2}(x)\, v_2^{(n)}(x) \right]^{(n-1-r)} \right]_{b+0}^{\ell} + \\ & + \sum_{n=0}^{\kappa} \int_0^b u_1^{(n)}(x) f_n(x) v_1^{(n)}(x)\,\mathrm{d}x + \sum_{n=0}^{\kappa} \int_b^\ell u_2^{(n)}(x) f_n(x) v_2^{(n)}(x)\,\mathrm{d}x = \\ & = K_0(u, v) + \sum_{n=0}^{\kappa} \int_0^b u_1^{(n)}(x) f_n(x) v_1^{(n)}(x)\,\mathrm{d}x + \sum_{n=0}^{\kappa} \int_b^\ell u_2^{(n)}(x) f_n(x) v_2^{(n)}(x)\,\mathrm{d}x\,, \end{aligned} \tag{16a}$$

and

$$\begin{aligned} (u, v)_M = {} & \left[\sum_{n=0}^{\mu} \sum_{r=0}^{n-1} (-1)^{(n+r)} u_1^{(r)}(x) \left[g_{n1}(x)\, v_1^{(n)}(x) \right]^{(n-1-r)} \right]_0^{b-0} + \\ & + \left[\sum_{n=0}^{\mu} \sum_{r=0}^{n-1} (-1)^{(n+r)} u_2^{(r)}(x) \left[g_{n2}(x)\, v_2^{(n)}(x) \right]^{(n-1-r)} \right]_{b+0}^{\ell} + \end{aligned}$$

$$+\sum_{n=0}^{\mu}\int_0^b u_1^{(n)}(x)g_{n1}(x)v_1^{(n)}(x)\,\mathrm{d}x+\sum_{n=0}^{\mu}\int_b^{\ell} u_2^{(n)}(x)g_{n2}(x)v_2^{(n)}(x)\,\mathrm{d}x=$$

$$=M_0(u,v)+\sum_{n=0}^{\mu}\int_0^b u_1^{(n)}(x)g_{n1}(x)v_1^{(n)}(x)\,\mathrm{d}x+\sum_{n=0}^{\mu}\int_b^{\ell} u_2^{(n)}(x)g_{n2}(x)v_2^{(n)}(x)\,\mathrm{d}x. \tag{16b}$$

The expressions $K_0(u,v)$ and $M_0(u,v)$ are defined by the right sides of equations (16). They are referred to as boundary and continuity expressions. If

$$K_0(u,v)=K_0(v,u) \qquad \text{and} \qquad M_0(u,v)=M_0(v,u) \tag{17}$$

then the coupled eigenvalue problem determined by equations (15), (2) is obviously self-adjoint. The coupled eigenvalue problem is called simple if

$$M_1[y]=g_{01}(x)y_1(x) \qquad \text{and} \qquad M_2[y]=g_{02}(x)y_2(x). \tag{18}$$

Assume that the eigenvalue problem considered is simple. Assume further that the Green function that belongs to the coupled differential equations

$$K_i\left[y_i(x)\right]=r_i(x), \qquad i=1,2 \tag{19}$$

associated with boundary condition and continuity conditions (2) is known. Then it holds that

$$y(x)=\lambda\int_0^{\ell} G(x,\xi)g_0(\xi)y(\xi)\,\mathrm{d}\xi\,, \tag{20}$$

where

$$y(x)=\begin{cases} y_1(x) & \text{if } \xi\in[0,b)\,,\\ y_2(x) & \text{if } \xi\in(b,\ell] \end{cases} \qquad \text{and} \qquad g_0(x)=\begin{cases} g_{01}(x) & \text{if } \xi\in[0,b)\,,\\ g_{02}(x) & \text{if } \xi\in(b,\ell] \end{cases}$$

is the eigenfunction $y(x)$ that belong to the eigenvalue λ while the structure of $G(x,\xi)$ is given by (6). In this way the coupled eigenvalue problem is reduced to an eigenvalue problem governed by a homogeneous Fredholm integral equation. Assume that the original eigenvalue problem is self-adjoint and positive definite, i.e. it holds, among others, that $g_0(\xi)>0$ ($\xi\in[0,\ell]$). Under these conditions the previous Fredholm integral equation can be rewritten into the form

$$\mathcal{Y}(x)=\lambda\int_0^{\ell}\mathcal{K}(x,\xi)\mathcal{Y}(\xi)\,\mathrm{d}\xi\,, \tag{21}$$

where

$$\mathcal{Y}(x)=\sqrt{g_0(x)}y(x), \qquad \mathcal{K}(x,\xi)=\sqrt{g_0(x)}G(x,\xi)\sqrt{g_0(\xi)} \tag{22}$$

in which $\mathcal{Y}(x)$ is a new unknown function and the kernel $\mathcal{K}(x,\xi)$ is symmetric.

6. Stepped beams

6.1. **Governing equations for heterogeneous stepped beam problems.** Figure 2 shows a pinned-pinned heterogeneous stepped beam (PPStp beam). The axial force N ($N>0$) is compressive in this figure. The transverse coordinates are $\hat{y},\hat{z}$, while the longitudinal is $\hat{x}=\hat{\xi}$. The coordinate plane $\hat{x}\hat{z}$ is a symmetry plane of the beam.

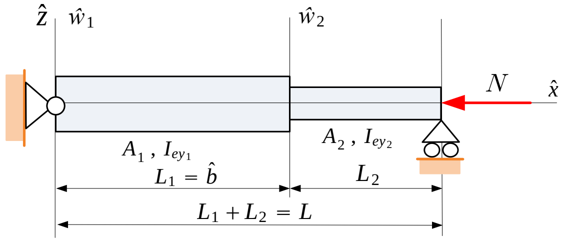

Figure 2. Heterogeneous stepped beam

The cross-sectional areas A_i, $(i = 1, 2)$ are constants. The beam is assumed to have heterogeneous cross sections, which means that the modulus of elasticity E satisfies the condition $E(\hat{y}, \hat{z}) = E(-\hat{y}, \hat{z})$. In this case we speak about cross-sectional heterogeneity. The length of the beam is L, the discontinuity in the cross sections is at $\hat{b}$. We should mention that the E-weighted first moment [19] $Q_{\hat{y}}$ is zero in this coordinate system:

$$Q_{\hat{y}} = \int_A \hat{z} E(\hat{y}, \hat{z}) \mathrm{d}A = 0\,. \tag{23}$$

The E-weighted moments of inertia [19] are defined by the equations

$$I_{ey_1} = \int_{A_1} E(\hat{y}, \hat{z}) z^2 \, \mathrm{d}A, \quad I_{ey_2} = \int_{A_2} E(\hat{y}, \hat{z}) z^2 \, \mathrm{d}A. \tag{24}$$

The beam is subjected to distributed forces $\hat{f}_{y1}(\hat{x})$, $\hat{x} \in [0, L_1)$, $\hat{f}_{y2}(\hat{x})$, $\hat{x} \in [(L_1, L]$ acting on the center line $\hat{x}$. The vertical displacements on the center line are denoted by $\hat{w}_1$, $\hat{x} \in [0, L_1)$ and $\hat{w}_2$, $\hat{x} \in [0, L_1)$.

In what follows we shall introduce the following dimensionless quantities:

$$\begin{gathered} x = \hat{x}/L, \qquad \xi = \hat{\xi}/L, \qquad w_i = \hat{w}_i \;\; L \; (i = 1, 2), \\ b = \hat{b}/L\,, \qquad \ell = \left. \frac{x}{L} \right|_{x=L} = 1\,., \end{gathered} \tag{25}$$

(a) Equilibrium problems of PPStp beams with cross-sectional heterogeneity are governed by the following differential equations [19]:

$$\begin{gathered} K_i(w_i(x)) = I_{ey_i} w_i^{(4)} = f_{zi}(x)\,, \quad f_{zi} = L^3 \hat{f}_{zi}, \quad x \in \begin{cases} [0, b) & \text{if } i = 1 \\ (b, \ell) & \text{if } i = 2 \end{cases} \\ \frac{\mathrm{d}^k w_i}{\mathrm{d}x^k} = w_i^{(k)}, \;\; (k = 1, \ldots, 4) \end{gathered} \tag{26}$$

ODEs $(26)_1$ are associated with the following boundary and continuity conditions:

$$w_1(0) = 0\,, \quad w_2^{(1)}(0) = 0\,; \qquad w_2(\ell) = 0\,, \quad w_2^{(2)}(\ell) = 0\,. \tag{27a}$$

$$w_1(b-0) = w_2(b+0) \qquad w_1^{(1)}(b-0) = w_2^{(1)}(b+0) \tag{27b}$$

$$I_{ey_1} w_1^{(2)}(b-0) = I_{ey_2} w_2^{(2)}(b+0) \qquad I_{ey_1} w_1^{(3)}(b-0) = I_{ey_2} w_2^{(3)}(b+0) \tag{27c}$$

ODEs $(26)_1$ with boundary and continuity conditions (27) constitute a coupled boundary value problem.

With the Green function that belongs to the coupled boundary value problem $(26)_1$, (27) solution for the dimensionless deflection $w(x)$ ($w(x) = w_1(x)$ if $x \in [0,b]$; $w(x) = w_2(x)$ if $x \in [b,\ell]$) is given by the following equation:

$$w(x) = \int_0^\ell G(x,\xi) f(\xi) \mathrm{d}\xi, \qquad f(\xi) = \begin{cases} f_{z1}(\xi) & \text{if } \xi \in [0,b], \\ f_{z2}(\xi) & \text{if } \xi \in [b,\ell]. \end{cases} \tag{28}$$

(b) Vibration problems of PPStp beams. As regards the free vibrations of PPStp beams it holds that

$$f(\xi) = \begin{cases} \rho_{a1} A_1 L^4 \omega^2 w_1(x) & \text{if } \xi \in [0,b], \\ \rho_{a2} A_2 L^4 \omega^2 w_2(x) & \text{if } \xi \in [b,\ell]. \end{cases} = \underbrace{\rho_{a1} A_1 L^4 \omega^2}_{\lambda} w(\xi) \begin{cases} 1 & \text{if } \xi \in [0,b], \\ \dfrac{\rho_{a2} A_2}{\rho_{a1} A_1} & \text{if } \xi \in [b,\ell]. \end{cases} \tag{29}$$

in which $w_i(x)$ is the dimensionless amplitude, ρ_{ai} is the average density on A_i, while ω stands for the circular frequency of the vibrations. With these notations the differential equations

$$\begin{aligned} K_1(w_1(x)) &= I_{ey_1} w_i^{(4)} = \underbrace{\rho_{a1} A_1 L^4 \omega^2}_{\lambda} w_1(x)\,, \\ K_2(w_1(x)) &= I_{ey_2} w_2^{(4)} = \lambda \frac{\rho_{a2} A_2}{\rho_{a1} A_1} w_2(x) \end{aligned} \tag{30}$$

are satisfied by $w_i(x)$. Differential equations (30) with the boundary and continuity conditions (27) determine a coupled eigenvalue problem for which λ is the eigenvalue. Recalling (28), we may conclude that this eigenvalue problem is governed by the homogeneous Fredholm integral equation

$$w(x) = \lambda \int_0^\ell G(x,\xi) w(\xi) \left\{ \begin{array}{ll} 1 & \text{if } \xi \in [0,b], \\ \dfrac{\rho_{a2} A_2}{\rho_{a1} A_1} & \text{if } \xi \in [b,\ell]. \end{array} \right\} \mathrm{d}\xi. \tag{31}$$

6.2. **Calculation of the Green function.**

6.2.1. *Particular solutions.* The linearly independent particular solutions of the differential equation $K_i(w_i(x)) = 0$ are very simple functions:

$$w_{11} = w_{12} = 1\,, \quad w_{21} = w_{22} = x\,, \quad w_{31} = w_{32} = x^2\,, \quad w_{41} = w_{42} = x^3\,. \tag{32}$$

6.2.2. *Calculations of the Green function if $\xi \in (0,b)$.* We shall assume that

$$\left.\begin{aligned} G_{11}(x,\xi) &= \sum_{m=1}^{4} (a_{mI}(\xi) + b_{mI}(\xi)) w_{1m}(x), \qquad x < \xi; \\ G_{11}(x,\xi) &= \sum_{m=1}^{4} (a_{mI}(\xi) - b_{mI}(\xi)) w_{1m}(x), \qquad x > \xi; \end{aligned}\right. \quad x \in [0,b] \tag{33a}$$

$$G_{21}(x,\xi) = \sum_{m=1}^{4} c_{mI}(\xi) w_{2m}(x), \qquad x \in [b,\ell] \tag{33b}$$

where the coefficients $a_{m1}(\xi), b_{m1}(\xi)$ and $c_{m1}(\xi)$ are unknown functions. This selection ensures the fulfillment of the following properties of the definition: 1. (ii) and 3. Fulfillment of Property 1. (i) leads to the following equation system:

$$\begin{bmatrix} 1 & \xi & \xi^2 & \xi^3 \\ 0 & 1 & 2\xi & 3\xi^2 \\ 0 & 0 & 2 & 6\xi \\ 0 & 0 & 0 & 6 \end{bmatrix} \begin{bmatrix} b_{11} \\ b_{21} \\ b_{31} \\ b_{41} \end{bmatrix} = \begin{bmatrix} 0 \\ 0 \\ 0 \\ -\frac{1}{2I_{ey_1}} \end{bmatrix} \tag{34}$$

from where

$$\begin{bmatrix} b_{11} \\ b_{21} \\ b_{31} \\ b_{41} \end{bmatrix} = \frac{1}{12 I_{ey_1}} \begin{bmatrix} \xi^3 \\ -3\xi^2 \\ 3\xi \\ -1 \end{bmatrix} . \tag{35}$$

Property 4 of the definition requires that the boundary and continuity conditions should all be satisfied. Therefore equations (27) yield the following equation system:
Boundary conditions at $x = 0$:

$$\sum_{m=1}^{4} a_{m1} w_{m1}(0) = -\sum_{m=1}^{4} b_{m1} w_{m1}(0)\,, \tag{36a}$$

$$\sum_{m=1}^{4} a_{m1} w_{m1}^{(2)}(0) = -\sum_{m=1}^{4} b_{m1} w_{m1}^{(2)}(0)\,. \tag{36b}$$

Continuity conditions at $x = b$:

$$\sum_{m=1}^{4} a_{m1} w_{m1}(b) - \sum_{m=1}^{4} c_{mi} w_{m2}(b) = \sum_{m=1}^{4} b_{m1} w_{m1}(b)\,, \tag{36c}$$

$$\sum_{m=1}^{4} a_{m1} w_{m1}^{(1)}(b) - \sum_{m=1}^{4} c_{mi} w_{m2}^{(1)}(b) = \sum_{m=1}^{4} b_{m1} w_{m1}^{(1)}(b)\,, \tag{36d}$$

$$\sum_{m=1}^{4} a_{m1} w_{m1}^{(2)}(b) - \underbrace{\frac{I_{ey_2}}{I_{ey_1}}}_{\alpha} \sum_{m=1}^{4} c_{mi} w_{m2}^{(2)}(b) = \sum_{m=1}^{4} b_{mi} w_{m1}^{(2)}(b)\,, \tag{36e}$$

$$\sum_{m=1}^{4} a_{m1} w_{m1}^{(3)}(b) - \underbrace{\frac{I_{ey_2}}{I_{ey_1}}}_{\alpha} \sum_{m=1}^{4} c_{mi} w_{m2}^{(3)}(b) = \sum_{m=1}^{4} b_{mi} w_{m1}^{(3)}(b)\,. \tag{36f}$$

Boundary conditions at $x = \ell$:

$$\sum_{m=1}^{4} c_{m1} w_{m2}(0) = 0\,, \tag{36g}$$

$$\sum_{m=1}^{4} c_{m1} w_{m2}^{(2)}(0) = 0\,. \tag{36h}$$

After substituting w_{m1}, w_{m2}, and b_{m1}, equation system (36) assumes the following matrix form:

$$\begin{bmatrix} 1 & 0 & 0 & 0 & 0 & 0 & 0 & 0 \\ 0 & 0 & 1 & 0 & 0 & 0 & 0 & 0 \\ 0 & b & 0 & b^3 & -1 & -b & -b^2 & -b^3 \\ 0 & 1 & 0 & 3b^2 & 0 & -1 & -2b & -3b^2 \\ 0 & 0 & 0 & 6b & 0 & 0 & -2\alpha & -6\alpha b \\ 0 & 0 & 0 & 6 & 0 & 0 & 0 & -6\alpha \\ 0 & 0 & 0 & 0 & 1 & \ell & \ell^2 & \ell^3 \\ 0 & 0 & 0 & 0 & 0 & 1 & 2\ell & 3\ell^2 \end{bmatrix} \begin{bmatrix} a_{11} \\ a_{21} \\ a_{31} \\ a_{41} \\ c_{11} \\ c_{21} \\ c_{31} \\ c_{41} \end{bmatrix} = \frac{1}{12 I_{ey_1}} \begin{bmatrix} -\xi^3 \\ -3\xi \\ 2\xi^3 - 3\xi^2 b + 6\xi b^2 - b^3 \\ -3\xi^2 + 12\xi b - 3b^2 \\ 12\xi - 6b \\ -6 \\ 0 \\ 0 \end{bmatrix} \tag{37}$$

Making use of the closed form solutions for a_{m1}, b_{m1} and c_{m1} $(m = 1, \ldots, 4)$, we get $G_{11}(x,\xi)$ and $G_{21}(x,\xi)$ from equations (33):

$$\begin{aligned} G_{11}(x,\xi) = \frac{1}{12 I_{ey_1}} \big\{ & (-\xi^3 \pm \xi^3) + \\ & + \left[\frac{\xi}{\alpha \ell^2} \left(4\,(\ell - b)^3 + \alpha \left(12\ell b\,(\ell - b) + 2\xi^2 \ell + 4b^3 - 3\xi \ell^2 \right) \right) \pm \left(-3\xi^2 \right) \right] x + \\ & + (-3\xi \pm 3\xi)\, x^2 + \left(-\frac{1}{\ell}\,(\ell - 2\xi) \pm (-1) \right) x^3 \Big\}, \end{aligned} \tag{38a}$$

$$G_{21}(x,\xi) = \frac{2\xi\,(\ell - x)}{12 I_{ey_1} \alpha \ell^2} \left(2x\ell^2 - 3\ell b^2 - x^2 \ell + 2b^3 + \alpha \left(3\ell b^2 - \xi^2 \ell - 2b^3 \right) \right). \tag{38b}$$

6.2.3. *Calculation of the Green function if $\xi \in (b, \ell)$:* In this case it is assumed that

$$G_{12}(x,\xi) = \sum_{m=1}^{4} c_{m2}(\xi) w_{m1}(x), \qquad x \in [0, b]; \tag{39a}$$

$$\left.\begin{aligned} G_{22}(x,\xi) &= \sum_{m=1}^{4} (a_{m2}(\xi) + b_{m2}(\xi)) w_{m2}(x), \qquad x \le \xi \\ G_{22}(x,\xi) &= \sum_{m=1}^{4} (a_{m2}(\xi) - b_{m2}(\xi)) w_{m2}(x), \qquad x \ge \xi \end{aligned}\right\} \quad x \in [b, \ell]; \tag{39b}$$

in which the coefficients $a_{m2}(\xi), b_{m2}(\xi)$, and $c_{m2}(\xi)$ are again the unknowns.

Recalling the calculation steps that resulted in solution (35), we obtain that

$$\begin{bmatrix} b_{12} \\ b_{22} \\ b_{32} \\ b_{42} \end{bmatrix} = \frac{1}{12I_{ey_2}} \begin{bmatrix} \xi^3 \\ -3\xi^2 \\ 3\xi \\ -1 \end{bmatrix}. \tag{40}$$

The boundary conditions at $x=0$, $x=\ell$ and the continuity conditions at $x=b$ – the calculations are based on equations (36) but the details are omitted – lead to the following equation system:

$$\begin{bmatrix} 1 & b & b^2 & b^3 & 0 & -b & 0 & -b^3 \\ 0 & 1 & 2b & 3b^2 & 0 & -1 & 0 & -3b^2 \\ 0 & 0 & 2\alpha & 6\alpha b & 0 & 0 & 0 & -6b \\ 0 & 0 & 0 & \alpha & 0 & 0 & 0 & -1 \\ 0 & 0 & 0 & 0 & 1 & 0 & 0 & 0 \\ 0 & 0 & 0 & 0 & 0 & 0 & 1 & 0 \\ 1 & \ell & \ell^2 & \ell^3 & 0 & 0 & 0 & 0 \\ 0 & 0 & 2 & 6\ell & 0 & 0 & 0 & 0 \end{bmatrix} \begin{bmatrix} a_{12} \\ a_{22} \\ a_{32} \\ a_{42} \\ c_{12} \\ c_{22} \\ c_{32} \\ c_{42} \end{bmatrix} = \frac{1}{12I_{ey_2}} \begin{bmatrix} -\xi^3+3b\xi^2-3b^2\xi+b^3 \\ 3\xi^2-6b\xi+3b^2 \\ \alpha\,(6b-6\xi) \\ \alpha \\ 0 \\ 0 \\ \xi^3-3\ell\xi^2+3\ell^2\xi-\ell^3 \\ 6\xi-6\ell \end{bmatrix} \tag{41}$$

Utilizing the closed form solutions for a_{m1}, b_{m1}, and c_{m1}, the following formulae are obtained for $G_{11}(x,\xi)$ and $G_{21}(x,\xi)$ from equations (39):

$$G_{12}(x,\xi) = \frac{2x\,(\ell-\xi)}{12I_{ey_2}\ell^2}\left(2\xi\ell^2-3\ell b^2-\xi^2\ell+2b^3+\alpha\left(3\ell b^2-2b^3-x^2\ell\right)\right), \tag{42a}$$

$$\begin{aligned} G_{22}(x,\xi) = {} & \frac{1}{12I_{ey_2}\ell}\left(4b^3\xi-\ell\xi^3-4\ell b^3+4\alpha b^3(\ell-\xi)\right) \pm \frac{\xi^3}{12I_{ey_2}} + \\ & + \left(\frac{1}{12I_{ey_2}\ell^2}\left(4\ell^3\xi+2\ell\xi^3-3\ell^2\xi^2-4b^3\xi+4\ell b^3+4b^3\alpha\xi-4\ell b^3\alpha\right) \pm \frac{-3\xi^2}{12I_{ey_2}}\right)x + \\ & + \left(\frac{-3\xi}{12I_{ey_2}} \pm \frac{3\xi}{12I_{ey_2}}\right)x^2 + \left(-\frac{1}{12I_{ey_2}\ell}(\ell-2\xi) \pm \frac{-1}{12I_{ey_2}}\right)x^3 \end{aligned} \tag{42b}$$

Remark 4. Recalling and applying then formula (16) to differential equations (26), we may conclude that $K_0(u,v)=0$ in (16). This means that the coupled boundary value problem defined by (16) and (27) is self-adjoint. Consequently the Green function should be symmetric, i.e., it holds that

$$G(x,\xi) = G(\xi,x).$$

It is clear from a comparison of (38b) and (42a) that $G_{12}(x,\xi) = G_{21}(\xi,x)$. It can also be checked by paper-and-pencil calculations that $G_{11}(x,\xi) = G_{11}(\xi,x)$ and $G_{22}(x,\xi) = G_{22}(\xi,x)$.

Remark 5. The unit of the Green function is $1/\mathrm{N\,mm}^2$.

Remark 6. Let us introduce the dimensionless distributed load

$$\mathfrak{f}_{zi} = \frac{f_{zi}}{I_{ey_i}} = \frac{L^3 \hat{f}_{zi}}{I_{ey_i}} \tag{43}$$

and multiply equations $(26)_1$ by $1/I_{ey_i}$. The result is

$$w_i^{(4)} = \mathfrak{f}_{zi}(x)\,. \tag{44}$$

Note that differential equations (44) with the boundary and continuity conditions (27) determine now a three-point boundary value problem – therefore the coupling has been removed. The dimensionless Green function for this three-point boundary value problem is given by the equation

$$\mathcal{G}(x,\xi) = \begin{cases} \mathcal{G}_{11}(x,\xi) = I_{ey_1} G_{11}(x,\xi) & \text{if } \ x,\xi \in [0,b], \\ \mathcal{G}_{21}(x,\xi) = I_{ey_1} G_{21}(x,\xi) & \text{if } \ x \in [b,\ell] \text{ and } \xi \in [0,b], \\ \mathcal{G}_{12}(x,\xi) = I_{ey_2} G_{12}(x,\xi) & \text{if } \ x \in [0,b] \text{ and } \xi \in [b,\ell], \\ \mathcal{G}_{22}(x,\xi) = I_{ey_2} G_{22}(x,\xi) & \text{if } \ x,\xi \in [b,\ell]. \end{cases} \tag{45}$$

It is worthy of mention that $\mathcal{G}(x,\xi)$ depends on I_{ey_1} and I_{ey_2} via α only, The presence of this parameter reflects the fact that the beam considered is stepped. The solution for the equilibrium problem is then

$$w(x) = \int_0^\ell \mathcal{G}(x,\xi)\mathfrak{f}(\xi)\mathrm{d}\xi, \qquad \mathfrak{f}(\xi) = \begin{cases} \mathfrak{f}_{z1}(\xi) & \text{if } \ \xi \in [0,b], \\ \mathfrak{f}_{z2}(\xi) & \text{if } \ \xi \in [b,\ell]. \end{cases}$$

Though the three-point boundary value problem (44), (27) is not self-adjoint, the following symmetry conditions are obviously satisfied:

$$\begin{cases} \mathcal{G}_{11}(x,\xi) = \mathcal{G}_{11}(\xi,x) & \text{if } \ x,\xi \in [0,b], \\ \frac{\mathcal{G}_{21}(x,\xi)}{I_{ey1}} = \frac{\mathcal{G}_{12}(\xi,x)}{I_{ey2}} & \text{if } \ x \in [b,\ell] \text{ and } \xi \in [0,b], \\ \mathcal{G}_{22}(x,\xi) = \mathcal{G}_{22}(\xi,x) & \text{if } \ x,\xi \in [b,\ell]. \end{cases} \tag{46}$$

If we write $\hat{b}$, L, $\hat{x}$ and $\hat{\xi}$ for b, ℓ, x and ξ in formulate (45) we obtain the Green function for the case when we use a selected length unit. Then the unit of the Green function is the cube of the length unit selected.

For the purpose of displaying the behavior of the Green function, Figure 3 depicts then graph when $L = 100$ mm, $\hat{b} = 50$ mm, $\hat{\xi} = 75$ mm and $\alpha = 0.52200625$.

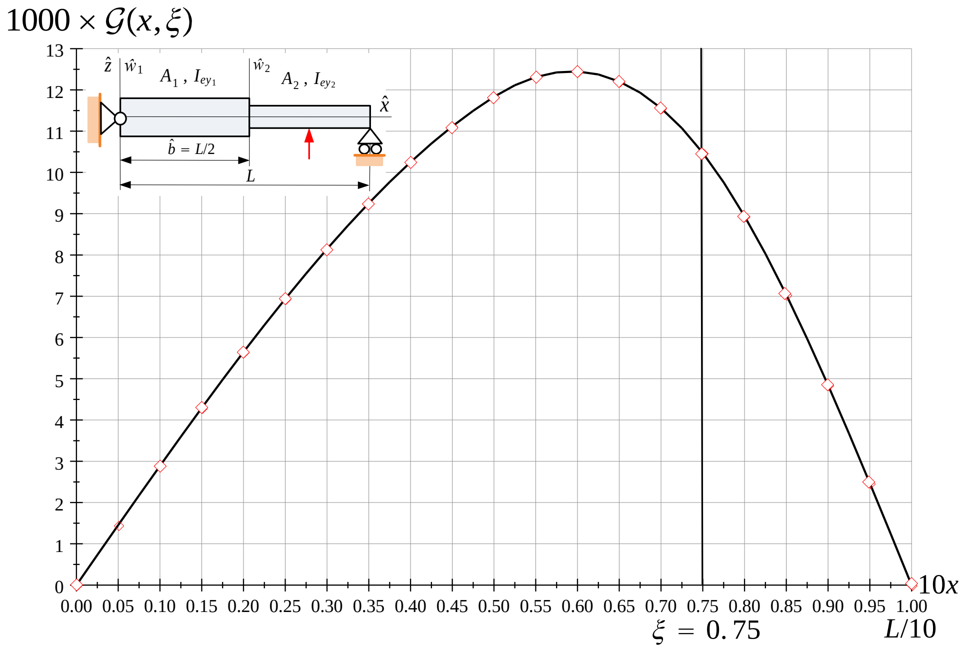

Figure 3. The Green function of a PPStp beam

Remark 7. With (45) the eigenvalue problem (31) for λ can be rewritten into the following form

$$w(x) = \chi \int_0^\ell \mathcal{G}(x,\xi)w(\xi) \left\{ \begin{array}{ll} 1 & \text{if } \xi \in [0,b], \\ \kappa & \text{if } \xi \in [b,\ell]. \end{array} \right\} \mathrm{d}\xi\,, \tag{47}$$

where

$$\chi = \frac{\lambda}{I_{ey_1}} = \frac{\rho_{a1}A_1L^4}{I_{ey_1}}\omega^2, \qquad \text{and} \qquad \kappa = \frac{\rho_{a2}A_2I_{ey_1}}{\rho_{a1}A_1I_{ey_2}} \tag{48}$$

is the new eigenvalue.

6.3. **Example 1.** Consider the stepped beam shown in Figure 4. We shall assume that $\nu = 0.95, 0.90, 0.85, 0.80, 0.75$ if $\hat{x} \in (\hat{b}, L]$. It is also assumed that $D_1 = 50\,\mathrm{mm}$, while $E_1 = E_2 = E_{steel} = 2.0 \times 10^5\,\mathrm{N/mm}^2$. The length L of the beam is 800 mm, the location of the middle support is given by the parameter $\hat{b}$. The surface densities have the following values: $\rho_1 = \rho_2 = \rho_{\text{steel}} = 7850\ \ \mathrm{kg}/10^9\mathrm{mm}^3$. Under the previous conditions Table 1 shows the characteristic data for the various cross sections.

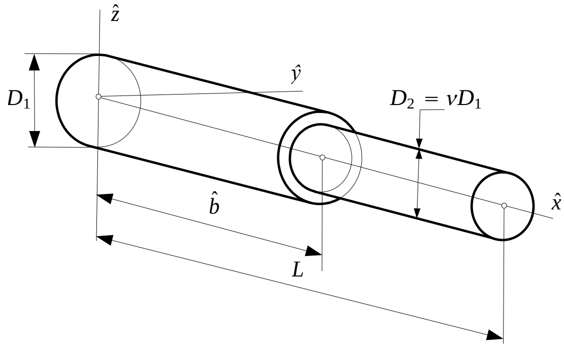

Figure 4. Stepped beam with circular cross section

Table 1. Data for the cross sections

ν	$\rho_a = \rho_1 = \rho_2$ kg/mm^3	$I_{ey1} \times 10^{-13}$ kg mm$^3/s^2$	$I_{ey2} \times 10^{-13}$ kg mm$^3/s^2$	α	κ
0.95			4.997747756	0.81450625	1.052631579
0.90			4.025779180	0.65610000	1.234586718
0.85	7.850×10^{-6}	6.135923152	3.202990235	0.52200625	1.384099617
0.80			2.513274123	0.40960000	1.562500000
0.75			1.473235149	0.31640625	1.777777778

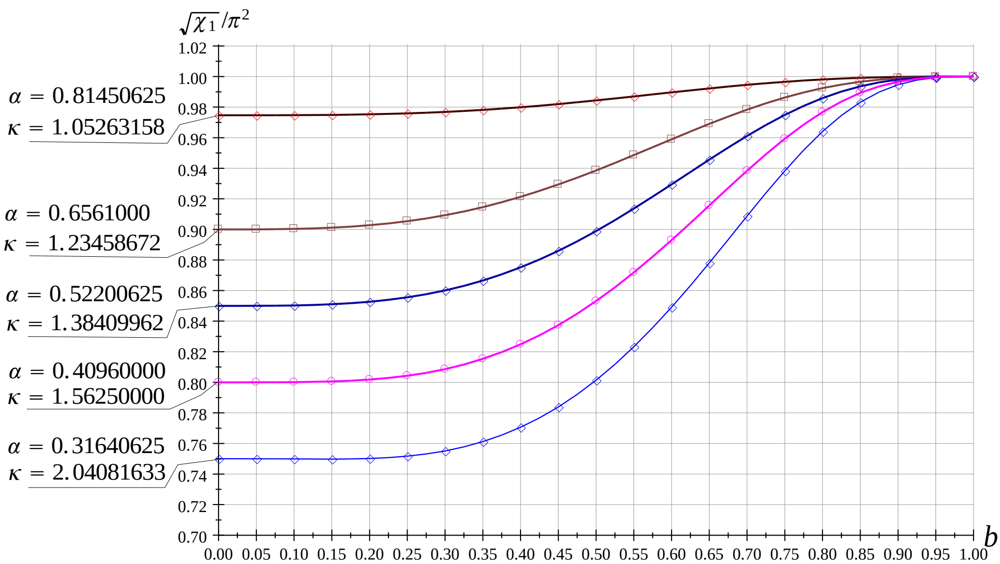

Figure 5. The first eigenvalue as a function of b; α and κ are parameters

The eigenvalue problem (47)–(48) is solved numerically by using a solution algorithm based on the boundary element method and published in [17].

Figure 5 shows the computational results for $\sqrt{\chi_1}/4.73004^2$ as a function of the dimensionless parameter b. Each curve in Figure 5 corresponds to a different value of the parameter α.

Assume that $b = 0.5$. If $\nu = 0.8$ we have $\alpha = 0.4096$ and $\kappa = 1.562\,5$. It follows from equation (48) that

$$\omega_1 = \frac{1}{L^2}\sqrt{\frac{I_{ey_1}}{\rho_{a1}A_1}\chi_1} = \frac{1}{800^2} \times \left(\sqrt{\frac{6.135\,923\,152 \times 10^{13}}{7.850 \times 10^{-6} \times 25^2 \times \pi}}\right) \times 8.420\,160\,122 = \\ = 830.100\,277\,1 \ \ \text{r/sec.} \quad (49)$$

If there is no step in the beam

$$\sqrt{\chi_1} = \pi^2 \times 1.0 = 9.869\,604\,4019.$$

and

$$\omega_1 = \frac{1}{800^2} \times \left(\sqrt{\frac{6.135\,923\,152 \times 10^{13}}{7.850 \times 10^{-6} \times 25^2 \times \pi}}\right) \times 9.869\,604\,4019 = 972.993\,533\,4 \ \ \text{r/sec.}$$

These results are compared with finite element calculations using Ansys. For mesh generation, a total of 360 uniform hexahedral elements (SOLID185) were used to discretize the geometry. A good agreement has been found:

Table 2. Comparison to FEM results

Eigenfrequency (Hz)	Our solution	Ansys solution	Relative error
Stepped beam	$\frac{830.100\,277\,1}{2\pi} = 132.115$	131.18	0.707%
Unifrom beam	$\frac{972.\,993\,53}{2\pi} = 154.\,865$	154.15	0.462%

When calculating the relative error our solution was the denominator.

7. Axially loaded stepped beams

7.1. **Governing equations.** We shall consider three different problems for axially loaded heterogeneous beams.

(a) Equilibrium problems. If a PPStp beam with cross-sectional heterogeneity is axially loaded, equilibrium problems are governed by the ODEs

$$\begin{aligned} K_{1a}(w_1(x)) &= I_{ey_1} w_1^{(4)} \pm N_1 L^2 w_1^{(2)} = f_{z1}(x), \ \ x \in [0, b]; \\ K_{2a}(w_2(x)) &= I_{ey_2} w_2^{(4)} \pm N_2 L^2 w_2^{(2)} = f_{z2}(\hat{x}), \ \ x \in [b, l], \end{aligned} \quad (50)$$

where N_1 and N_2 ($N_1 > 0$, $N_2 > 0$) are the axial forces acting on the beam. Their signs are (positive) [negative] if the considered axial force is (compressive) [tensile]. ODEs (50) are associated with boundary and continuity conditions (27). Note that boundary value problem (50), (27) is again a coupled boundary value problem.

In the sequel we shall assume that $N_1 = N_2 = N$.

If we know the Green functions $G = G_c(x,\xi)$ (N is compressive) and $G = G_t(x,\xi)$ (N is tensile) solution for the dimensionless deflection $w(x)$ ($w(x) = w_1(x)$ if $x \in [0,b]$; $w(x) = w_2(x)$ if $x \in [b,\ell]$) is given by integral (28) in which ($G(x,\xi) = G_c(x,\xi)$ if the axial force is compressive) $[G(x,\xi) = G_t(x,\xi)$ if the axial force is tensile$]$.

REMARK 8. It can be checked with ease that the coupled boundary value problem (50), (27) is self-adjoint.

(b) Stability problems. If $f_{z1}(x) = f_{z2}(x) = 0$, $N_1 = N_2 = N$ and the sign of N is positive we get

$$\begin{aligned} K_{1as}(w_1(x)) &= w_1^{(4)} + \mathcal{N}_1 w_1^{(2)} = 0, \quad \mathcal{N}_1 = \frac{NL^2}{I_{ey_1}}, \quad x \in [0,b]; \\ K_{2as}(w_2(x)) &= w_2^{(4)} + \mathcal{N}_2 w_2^{(2)} = 0, \quad \mathcal{N}_2 = \frac{NL^2}{I_{ey_2}}, \quad x \in [b,l]. \end{aligned} \tag{51}$$

ODEs (51) with boundary and continuity conditions (27) constitute a coupled eigenvalue problem for which N is the eigenvalue sought. This problem is solved in Appendix A.

(c) Vibration problems. If the axially loaded beams vibrate, the amplitudes should fulfill ODEs

$$\begin{aligned} K_{1av}(w_1(x)) &= w_1^{(4)} \pm \mathcal{N}_1 w_1^{(2)} = \chi w_1, \quad \chi = \frac{\lambda}{I_{ey_1}} = \frac{\rho_{a1} A_1 L^4 \omega^2}{I_{ey_1}}, \quad x \in [0,b]; \\ K_{2av}(w_2(x)) &= w_2^{(4)} \pm \mathcal{N}_2 w_2^{(2)} = \chi\kappa w_2, \quad \chi\kappa = \frac{\rho_{a2} A_2 L^4 \omega^2}{I_{ey_2}}, \quad x \in [b,l], \end{aligned} \tag{52}$$

which are associated with boundary and continuity conditions (27). ODEs (52) with boundary and continuity conditions (27) constitute a coupled eigenvalue problem with χ as the eigenvalue.

7.2. **Calculation of the Green function for compressive axial force.** Let us introduce the quantities

$$p_1 = \sqrt{\mathcal{N}_1}, \qquad p_2 = \sqrt{\mathcal{N}_2} = p_1\sqrt{\alpha}. \tag{53}$$

With (53), solutions to the dimensionless displacements in equations (50) – the signs of $N_1 L^2 w_1^{(2)}$ and $N_2 L^2 w_2^{(2)}$ are positive – are given by

$$w_1 = \sum_{\ell=1}^{4} a_{\ell 1} w_{\ell 1}(x) = a_{11} + a_{21}x + a_{31}\cos p_1 x + a_{41}\sin p_1 x, \qquad p_1 = \sqrt{\mathcal{N}_1}; \tag{54a}$$

$$w_2 = \sum_{\ell=1}^{4} a_{\ell 2} w_{\ell 2}(x) = a_{12} + a_{22}x + a_{32}\cos p_2 x + a_{42}\sin p_2 x, \qquad p_2 = \sqrt{\mathcal{N}_2}. \tag{54b}$$

The structure of the Green function is presented by equation (6).
If $\xi \in (0,b)$ we shall assume that

$$\begin{aligned} G_{c11}(x,\xi) &= \sum_{m=1}^{4}(a_{m1}(\xi)+b_{m1}(\xi))w_{1m}(x), \qquad x<\xi \\ & \qquad\qquad\qquad\qquad\qquad\qquad\qquad x\in[0,b] \\ G_{c11}(x,\xi) &= \sum_{m=1}^{4}(a_{m1}(\xi)-b_{m1}(\xi))w_{1m}(x), \qquad x>\xi \end{aligned} \tag{55a}$$

$$G_{c21}(x,\xi)=\sum_{m=1}^{4}c_{m1}(\xi)w_{2m}(x). \qquad x\in[b,\ell] \tag{55b}$$

Here, the coefficients $a_{m1}(\xi), b_{m1}(\xi)$, and $c_{m1}(\xi)$ are the unknown functions. If we follow the calculation steps detailed in Subsection 6.2.2 we get the equation systems:

$$\begin{bmatrix} 1 & \xi & \cos p_1\xi & \sin p_1\xi \\ 0 & 1 & -p_1\sin p_1\xi & p_1\cos p_1\xi \\ 0 & 0 & -p_1^2\cos p_1\xi & -p_1^2\sin p_1\xi \\ 0 & 0 & p_1^3\sin p_1\xi & -p_1^3\cos p_1\xi \end{bmatrix}\begin{bmatrix} b_1\\ b_2\\ b_3\\ b_4\end{bmatrix}=\begin{bmatrix}0\\0\\0\\ \frac{-1}{2I_{ey_1}}\end{bmatrix}, \qquad \begin{bmatrix} b_1\\ b_2\\ b_3\\ b_4\end{bmatrix}=\frac{1}{2I_{ey_1}}\begin{bmatrix}\frac{\xi}{p_1^2}\\ -\frac{1}{p_1^2}\\ -\frac{\sin p_1\xi}{p_1^3}\\ \frac{\cos p_1\xi}{p_1^3}\end{bmatrix} \tag{56}$$

and

$$\begin{bmatrix} 1 & 0 & 1 & 0 & 0 & 0 & 0 & 0 \\ 0 & 0 & 1 & 0 & 0 & 0 & 0 & 0 \\ 1 & b & \cos p_1 b & \sin p_1 b & -1 & -b & -\cos p_2 b & -\sin p_2 b \\ 0 & 1 & -p_1\sin p_1 b & p_1\cos p_1 b & 0 & -1 & p_2\sin p_2 b & -p_2\cos p_2 b \\ 0 & 0 & -p_1^2\cos p_1 b & -p_1^2\sin p_1 b & 0 & 0 & \alpha p_2^2\cos p_2 b & \alpha p_2^2\sin p_2 b \\ 0 & 0 & p_1^3\sin p_1 b & -p_1^3\cos p_1 b & 0 & 0 & -\alpha p_2^3\sin p_2 b & \alpha p_2^3\cos p_2 b \\ 0 & 0 & 0 & 0 & 1 & \ell & \cos p_2\ell & \sin p_2\ell \\ 0 & 0 & 0 & 0 & 0 & 0 & \cos p_2\ell & \sin p_2\ell \end{bmatrix}\begin{bmatrix} a_{1I}\\ a_{2I}\\ a_{3I}\\ a_{4I}\\ c_{1I}\\ c_{2I}\\ c_{3I}\\ c_{4I}\end{bmatrix}=$$

$$=\frac{1}{2I_{ey_1}p_1^3}\begin{bmatrix} -p_1\xi+\sin p_1\xi \\ \sin p_1\xi \\ p_1\xi-p_1 b+\sin p_1(b-\xi) \\ -p_1+p_1\cos p_1(b-\xi) \\ -p_1^2\sin p_1(b-\xi) \\ -p_1^3\cos p_1(\xi-b) \\ 0 \\ 0 \end{bmatrix} \tag{57}$$

If $\xi \in (b,\ell)$ it is assumed that

$$\begin{aligned} G_{c22}(x,\xi) &= \sum_{m=1}^{4}(a_{m2}(\xi)+b_{m2}(\xi))w_{2m}(x), \qquad x<\xi \\ & \qquad\qquad\qquad\qquad\qquad\qquad\qquad x\in[b,\ell] \\ G_{c22}(x,\xi) &= \sum_{m=1}^{4}(a_{m2}(\xi)-b_{m2I}(\xi))w_{2m}(x), \qquad x>\xi \end{aligned} \tag{58a}$$

$$G_{c12}(x,\xi)=\sum_{m=1}^{4}c_{m2}(\xi)w_{1m}(x), \qquad x\in[0,b] \tag{58b}$$

where the coefficients $a_{m2}(\xi), b_{m2}(\xi)$ and $c_{m2}(\xi)$ are the unknowns. By repeating the calculation steps presented in Subsection 6.2.3 the following equation system can be obtained for these unknown coefficients:

$$\begin{bmatrix} 1 & \xi & \cos p_2\xi & \sin p_2\xi \\ 0 & 1 & -p_2\sin p_2\xi & p_2\cos p_2\xi \\ 0 & 0 & -p_2^2\cos p_2\xi & -p_2^2\sin p_2\xi \\ 0 & 0 & p_2^3\sin p_2\xi & -p_2^3\cos p_2\xi \end{bmatrix} \begin{bmatrix} b_1 \\ b_2 \\ b_3 \\ b_4 \end{bmatrix} = \begin{bmatrix} 0 \\ 0 \\ 0 \\ \frac{-1}{2I_{ey_1}} \end{bmatrix}, \quad \begin{bmatrix} b_{1II} \\ b_{2II} \\ b_{3II} \\ b_{4II} \end{bmatrix} = \frac{1}{2I_{ey_1}} \begin{bmatrix} \frac{\xi}{p_2^2} \\ -\frac{1}{p_2^2} \\ -\frac{\sin p_2\xi}{p_2^3} \\ \frac{\cos p_2\xi}{p_2^3} \end{bmatrix} \tag{59}$$

and

$$\begin{bmatrix} 1 & b & \cos p_2b & \sin p_2b & 0 & -b & 0 & -\sin p_1b \\ 0 & 1 & -p_2\sin p_2b & p_2\cos p_2b & 0 & -1 & 0 & -p_1\cos p_1b \\ 0 & 0 & -\alpha p_2^2\cos p_2b & -\alpha p_2^2\sin p_2b & 0 & 0 & 0 & p_1^2\sin p_1b \\ 0 & 0 & \alpha p_2^3\sin p_2b & -\alpha p_2^3\cos p_2b & 0 & 0 & 0 & p_1^3\cos p_1b \\ 0 & 0 & 0 & 0 & 1 & 0 & 0 & 0 \\ 0 & 0 & 0 & 0 & 0 & 0 & 1 & 0 \\ 1 & \ell & \cos p_2\ell & \sin p_2\ell & 0 & 0 & 0 & 0 \\ 0 & 0 & -\cos p_2\ell & -\sin p_2\ell & 0 & 0 & 0 & 0 \end{bmatrix} \begin{bmatrix} a_{1II} \\ a_{2II} \\ a_{3II} \\ a_{4II} \\ c_{1II} \\ c_{2II} \\ c_{3II} \\ c_{4II} \end{bmatrix} =$$

$$= -\frac{1}{2I_{ey_2}p_2^3} \begin{bmatrix} p_2\xi - p_2b + \sin p_2(b-\xi) \\ p_2\cos p_2(b-\xi) - p_2 \\ -\alpha p_2^2\sin p_2(b-\xi) \\ -\alpha p_2^3\cos p_2(b-\xi) \\ 0 \\ 0 \\ -p_2\xi + p_2\ell - \sin p_2(\ell-\xi) \\ \sin p_2(\ell-\xi) \end{bmatrix} \tag{60}$$

The closed form solutions for $a_{11}(\xi), \ldots, c_{42}(\xi)$ obtained by solving equations (57) and (60) are very long formulae and for this reason they are not presented here.

Remark 9. The Green function $G_c(x\xi)$ is symmetric, i.e., it holds that $G_c(x,\xi) = G_c(\xi,\xi)$. Fulfillment of the symmetry condition is checked by numerical computations since the paper-and-pencil calculations for checking the symmetry condition are very time consuming.

Remark 10. The dimensionless Green functions $\mathcal{G}_c(x,\xi)$ can be calculated by using equation (45). $\mathcal{G}_c(x,\xi)$ fulfills symmetry conditions (46).

Remark 11. Assume that $b = 0.5$, $\xi = 0.75$ and $\alpha = 0.52200625$. Then the critical value of the dimensionless compressive force p_2 is equal to 3.55896485 – see Figure 8. Under these conditions, Figure 6 depicts the Green function $\mathcal{G}(x,\xi)$.

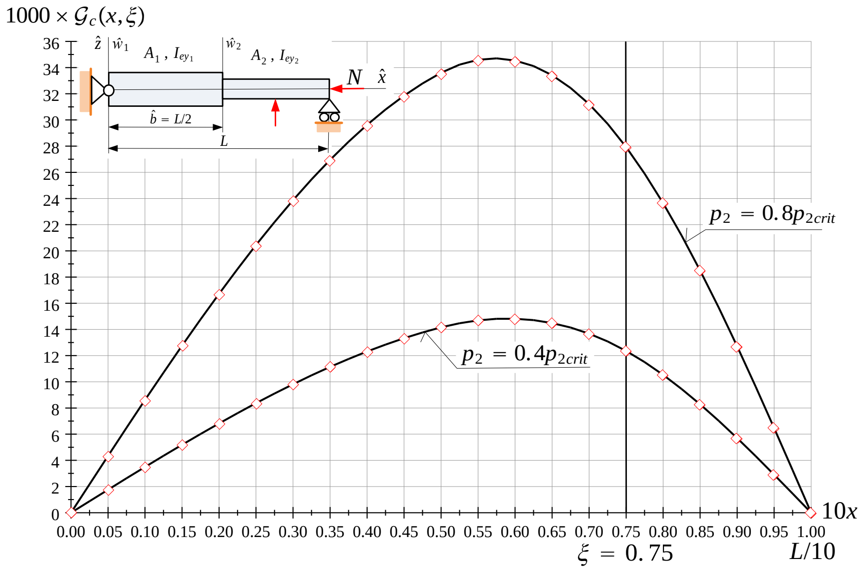

Figure 6. The Green function of a PPStp beam subjected to a compressive force

7.3. **Calculation of the Green function for tensile axial force.** Recalling equations (50), solutions to the dimensionless displacements – the signs of $N_1L^2w_1^{(2)}$ and $N_2L^2w_2^{(2)}$ is negative – are given by

$$w_1 = \sum_{\ell=1}^{4} a_{\ell 1}w_{\ell 1}(x) = a_{11} + a_{21}x + a_{31}\cosh p_1x + a_{41}\sinh p_1x, \tag{61a}$$

$$w_2 = \sum_{\ell=1}^{4} a_{\ell 2}w_{\ell 2}(x) = a_{12} + a_{22}x + a_{32}\cosh p_2x + a_{42}\sinh p_2x. \tag{61b}$$

The structure of the Green function is the same as earlier - see equations (6).
If $\xi \in (0, b)$ it is assumed that

$$\left.\begin{aligned} G_{t11}(x,\xi) &= \sum_{m=1}^{4}(a_{m1}(\xi) + b_{m1}(\xi))w_{1m}(x), \qquad x < \xi \\ G_{t11}(x,\xi) &= \sum_{m=1}^{4}(a_{m1}(\xi) - b_{m1}(\xi))w_{1m}(x), \qquad x > \xi \end{aligned}\right\} \quad x \in [0,b]; \tag{62a}$$

$$G_{t21}(x,\xi) = \sum_{m=1}^{4} c_{m1}(\xi)w_{2m}(x), \qquad x \in [b,\ell] \tag{62b}$$

where the coefficients $a_{m1}(\xi), b_{m1}(\xi)$ and $c_{m1}(\xi)$ are again the unknown functions. Application of the calculation steps detailed in Subsection 6.2.2 yields

$$\begin{bmatrix} 1 & \xi & \cosh p_1\xi & \sinh p_1\xi \\ 0 & 1 & p_1 \sinh p_1\xi & p_1 \cosh p_1\xi \\ 0 & 0 & p_1^2 \cosh p_1\xi & p_1^2 \sinh p_1\xi \\ 0 & 0 & p_1^3 \sinh p_1\xi & p_1^3 \cosh p_1\xi \end{bmatrix} \begin{bmatrix} b_1 \\ b_2 \\ b_3 \\ b_4 \end{bmatrix} = \begin{bmatrix} 0 \\ 0 \\ 0 \\ -\frac{1}{2} \end{bmatrix}, \quad \begin{bmatrix} b_1 \\ b_2 \\ b_3 \\ b_4 \end{bmatrix} = \frac{1}{2I_{ey_1}} \begin{bmatrix} -\frac{\xi}{p_1^2} \\ \frac{1}{p_1^2} \\ \frac{\sinh p_1\xi}{p_1^3} \\ -\frac{\cosh p_1\xi}{p_1^3} \end{bmatrix} \tag{63}$$

and

$$\begin{bmatrix} 1 & 0 & 1 & 0 & 0 & 0 & 0 & 0 \\ 0 & 0 & 1 & 0 & 0 & 0 & 0 & 0 \\ 1 & b & \cosh p_1 b & \sinh p_1 b & -1 & -b & -\cosh p_2 b & -\sinh p_2 b \\ 0 & 1 & p_1 \sinh p_1 b & p_1 \cosh p_1 b & 0 & -1 & -p_2 \sinh p_2 b & -p_2 \cosh p_2 b \\ 0 & 0 & p_1^2 \cosh p_1 b & p_1^2 \cosh p_1 b & 0 & 0 & -\alpha p_2^2 \cosh p_2 b & -\alpha p_2^2 \sinh p_2 b \\ 0 & 0 & p_1^3 \sinh p_1 b & p_1^3 \cosh p_1 b & 0 & 0 & -\alpha p_2^3 \sinh p_2 b & -\alpha p_2^3 \cosh p_2 b \\ 0 & 0 & 0 & 0 & 1 & \ell & \cosh p_2\ell & \sinh p_2\ell \\ 0 & 0 & 0 & 0 & 0 & 0 & \cosh p_2\ell & \sinh p_2\ell \end{bmatrix} \begin{bmatrix} a_{1I} \\ a_{2I} \\ a_{3I} \\ a_{4I} \\ c_{1I} \\ c_{2I} \\ c_{3I} \\ c_{4I} \end{bmatrix} =$$

$$= \frac{1}{2I_{ey_1} p_1^3} \begin{bmatrix} p_1\xi - \sinh p_1\xi \\ -\sinh p_1\xi \\ -p_1\xi + p_1 b - \sinh p_1 (b-\xi) \\ p_1 - p_1 \cosh p_1 (b-\xi) \\ -p_1^2 \sinh p_1 (b-\xi) \\ -p_1^3 \cosh p_1 (b-\xi) \\ 0 \\ 0 \end{bmatrix} \tag{64}$$

If $\xi \in (b, \ell)$ we shall assume that:

$$\begin{aligned} G_{t22}(x,\xi) &= \sum_{m=1}^{4} (a_{m2}(\xi) + b_{m2}(\xi)) w_{2m}(x), \qquad x < \xi \\ G_{t22}(x,\xi) &= \sum_{m=1}^{4} (a_{m2}(\xi) - b_{m2I}(\xi)) w_{2m}(x), \qquad x > \xi \end{aligned} \qquad x \in [b, \ell] \tag{65a}$$

$$G_{t12}(x,\xi) = \sum_{m=1}^{4} c_{m2}(\xi) w_{1m}(x). \qquad x \in [0, b] \tag{65b}$$

Recalling the the calculation steps presented in Subsection 6.2.3 we obtain the following equation systems

$$\begin{bmatrix} 1 & \xi & \cosh p_2\xi & \sinh p_2\xi \\ 0 & 1 & p_2 \sinh p_2\xi & p_2 \cosh p_2\xi \\ 0 & 0 & p_2^2 \cosh p_2\xi & p_2^2 \sinh p_2\xi \\ 0 & 0 & p_2^3 \sinh p_2\xi & p_2^3 \cosh p_2\xi \end{bmatrix} \begin{bmatrix} b_1 \\ b_2 \\ b_3 \\ b_4 \end{bmatrix} = \begin{bmatrix} 0 \\ 0 \\ 0 \\ -\frac{1}{2I_{ey_2}} \end{bmatrix}, \quad \begin{bmatrix} b_{1II} \\ b_{2II} \\ b_{3II} \\ b_{4II} \end{bmatrix} = \frac{1}{2I_{ey_2}} \begin{bmatrix} -\frac{\xi}{p_2^2} \\ \frac{1}{p_2^2} \\ \frac{\sinh p_2\xi}{p_2^3} \\ -\frac{\cosh p_2\xi}{p_2^3} \end{bmatrix} \tag{66}$$

and

$$\begin{bmatrix} 1 & b & \cosh p_2 b & \sinh p_2 b & 0 & -b & 0 & -\sinh p_1 b \\ 0 & 1 & p_2 \sinh p_2 b & p_2 \cosh p_2 b & 0 & -1 & 0 & -p_1 \cosh p_1 b \\ 0 & 0 & \alpha p_2^2 \cosh p_2 b & \alpha p_2^2 \sinh p_2 b & 0 & 0 & 0 & -p_1^2 \sinh p_1 b \\ 0 & 0 & \alpha p_2^3 \sinh p_2 b & -\alpha p_2^3 \cosh p_2 b & 0 & 0 & 0 & -p_1^3 \cosh p_1 b \\ 0 & 0 & 0 & 0 & 1 & 0 & 0 & 0 \\ 0 & 0 & 0 & 0 & 0 & 0 & 1 & 0 \\ 1 & \ell & \cosh p_2 \ell & \sinh p_2 \ell & 0 & 0 & 0 & 0 \\ 0 & 0 & \cosh p_2 \ell & \sinh p_2 \ell & 0 & 0 & 0 & 0 \end{bmatrix} \begin{bmatrix} a_{1II} \\ a_{2II} \\ a_{3II} \\ a_{4II} \\ c_{1II} \\ c_{2II} \\ c_{3II} \\ c_{4II} \end{bmatrix} =$$

$$= \frac{1}{2p_2^3} \begin{bmatrix} p_2\xi - p_2 b + \sinh p_2 (b-\xi) \\ p_2 \cosh p_2 (b-\xi) - p_2 \\ \alpha p_2^2 \sinh p_2 (b-\xi) \\ \alpha p_2^3 \cosh p_2 (b-\xi) \\ 0 \\ 0 \\ -p_2\xi + p_2\ell - \sinh p_2 (\ell - \xi) \\ -\sinh p_2 (\ell-\xi) \end{bmatrix} \tag{67}$$

The closed form solutions for the unknown functions $a_{11}(\xi), \dots, c_{42}(\xi)$ obtained by solving equations (64) and (67) are again very long formulae and for this reason they are not presented here.

Remark 12. The Green function $G_t(x\xi)$ is symmetric, i.e., it satisfies the symmetry condition $G_t(x,\xi) = G_t(\xi,\xi)$. Fulfillment of the symmetry condition was verified by numerical computations.

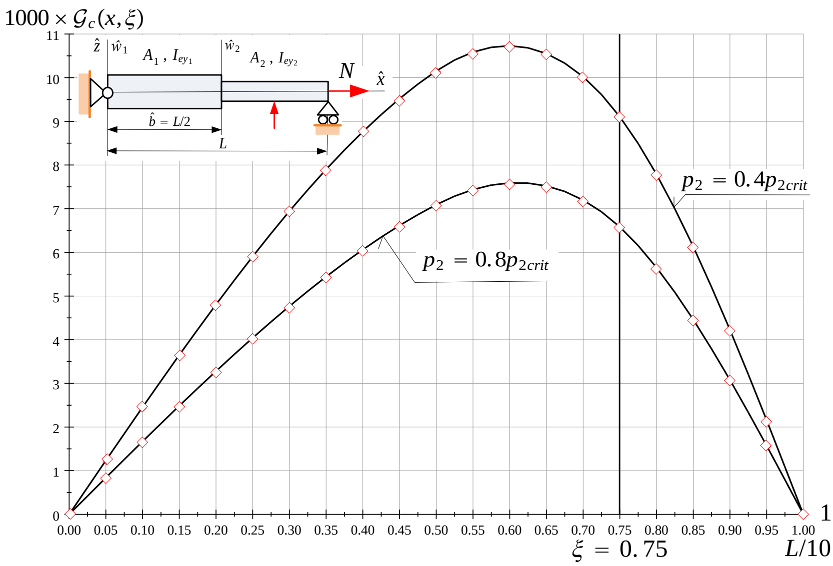

Figure 7. The Green function of a PPStp beam subjected to a tensile force

Remark 13. The dimensionless Green functions $\mathcal{G}_t(x,\xi)$ can be calculated by utilizing equation (45). $\mathcal{G}_t(x,\xi)$ fulfills the symmetry conditions (46).

Figure 7 shows the dimensionless Green function $\mathcal{G}_t(x,\xi)$ utilizing the data given in Remark 11.

Remark 14. It is clear from [Figure 6] {Figure 7} that the deflections are [greater] {smaller} if p_2 is [greater] {greater}. The fulfillment of these relationships is a natural requirement for the Green functions considered.

8. Axial load and eigenfrequencies of stepped beams

8.1. **Governing equations for the eigenvalue problem.** In this section it is our main objective to clarify the effect of the axial load on the eigenfrequencies of PPStp beams. Making use of the dimensionless Green functions the eigenvalue problems to be solved are governed by the homogeneous Fredholm integral equations for the case of a compressive force

$$w(x) = \chi \int_0^\ell \mathcal{G}_c(x,\xi) w(\xi) \left\{ \begin{array}{ll} 1 & \text{if } \xi \in [0,b], \\ \kappa & \text{if } \xi \in [b,\ell]. \end{array} \right\} \mathrm{d}\xi\,, \tag{68}$$

and for the case of a tensile force

$$w(x) = \chi \int_0^\ell \mathcal{G}_t(x,\xi) w(\xi) \left\{ \begin{array}{ll} 1 & \text{if } \xi \in [0,b], \\ \kappa & \text{if } \xi \in [b,\ell]. \end{array} \right\} \mathrm{d}\xi\,. \tag{69}$$

Here χ, i.e., the eigenvalue sought, and κ are given by equation (48). In the sequel we shall seek numerical solutions for the above problems utilizing the data related to the stepped beams that are considered in Subsection 6.3.

In the following, we shall need the value of the smallest critical force for the mentioned stepped beams. The solution to the corresponding eigenvalue problem is given in Appendix A – see Figure 8.

8.2. **Example 2.** Two problems are solved numerically. For the first problem it is assumed that $\nu = 0.90$; then $\alpha = 0.65610000$, and $\kappa = 1.234586718$. For the second problem $\nu = 0.80$, $\alpha = 0.40960000$, and $\kappa = 1.562500000$. These data are taken from Table 1. The first eigenfrequency and the critical force can be calculated by utilizing the data presented in Tables 3 and 4 – see Figures 5 and 8 for a comparison. Tables 3 and 4 contain some further data that are also utilized in the computations.

Table 3. Values of χ_1

	$\sqrt{\chi_1(b)}/\pi^2$				
ν	$b = 0.2$	$b = 0.4$	$b = 0.5$	$b = 0.6$	$b = 0.8$
0.9	0.90273411	0.92130879	0.93858272	0.95892739	0.99240078
0.8	0.80179239	0.82483041	0.85314059	0.89300215	0.97673594

Table 4. Critical force

	$\sqrt{N_{2\,\mathrm{crit}}}(b)$				
ν	$b=0.2$	$b=0.4$	$b=0.5$	$b=0.6$	$b=0.8$
0.9	3.16728280	3.30994880	3.43419178	3.58174237	3.82743853
0.8	3.18497550	3.43128449	3.66658411	3.98927283	4.72167938

Let us denote the first eigenfrequency for [compression] {tension} by [ω_{1c}] {ω_{1t}}. The first eigenfrequency of the unloaded beam is ω_1.

Tables 5–9 contain the computed results for Problem 1, 10–14 for Problem 2. In both cases the values of b are 0.2, 0.4, 0.5, 0.6, and 0.8. The first column in each table is a list of the values the quotient $\mathcal{N}_2/\mathcal{N}_{2crit}$ has, the second and fourth columns contain those values of ω_{1c} and ω_{1t} which belong to $\mathcal{N}_2/\mathcal{N}_{2crit}$. The third and fifth columns show the differences between two consecutive values of ω_{1c} and ω_{1t}. If these differences are constants then the functions $\omega_{1c}(\mathcal{N}_2/\mathcal{N}_{2crit})$ and $\omega_{1t}(\mathcal{N}_2/\mathcal{N}_{2crit})$ are in principle linear functions.

Each table is followed by two equations. The first is a quadratic approximation of the function $\omega_{1c}(\mathcal{N}_2/\mathcal{N}_{2crit})$, the second is a quadratic approximation of the function $\omega_{1c}(\mathcal{N}_2/\mathcal{N}_{2crit})$. See equations (70)–(79) for details. The quadratic approximations fit to the values of these functions an accuracy of four to five digits.

8.2.1. *Solutions to Problem 1.*

Table 5. Computational results for $\nu=0.9$ and $b=0.2$

$N/N_{crit}=$ $\mathcal{N}_2/\mathcal{N}_{2crit}$	$\omega^2_{1c}/\omega^2_{1\text{ no load}}$	Differences	$\omega^2_{1t}/\omega^2_{1\text{ no load}}$	Differences
0.000	0.99985049		1.00014949	
0.100	0.90001388	0.09983661	1.09998352	0.09983402
0.200	0.80002506	0.09998882	1.19996457	0.09998105
0.300	0.70003341	0.09999164	1.29994325	0.09997868
0.400	0.60003881	0.09999461	1.39991964	0.09997640
0.500	0.50004109	0.09999771	1.49989385	0.09997421
0.600	0.40004012	0.10000098	1.59986595	0.09997210
0.700	0.30003571	0.10000441	1.69983602	0.09997007
0.800	0.20002769	0.10000802	1.79980415	0.09996812
0.900	0.10001586	0.10001183	1.89977039	0.09996624
1.000	0.00000000	0.10001586	1.99973481	0.09996443

The quadratic approximations fit to the data presented in Table 5 with four-digit accuracy.

$$\frac{\omega^2_{1c}}{\omega^2_{1\text{ no load}}}=-3.331\,337\,633\times10^{-4}\frac{\mathcal{N}^2_2}{\mathcal{N}^2_{2crit}}-0.999\,625\,6857\frac{\mathcal{N}_2}{\mathcal{N}_{2crit}}+0.999\,945\,6098, \tag{70a}$$

$$\frac{\omega^2_{1t}}{\omega^2_{1\text{ no load}}}=6.307\,884\,335\times10^{-5}\frac{\mathcal{N}^2_2}{\mathcal{N}^2_{2crit}}+0.999\,631\,7373\frac{\mathcal{N}_2}{\mathcal{N}_{2crit}}+1.000\,053\,866. \tag{70b}$$

Table 6. Computational results for $\nu = 0.9$ and $b = 0.4$

$N/N_{crit} = \mathcal{N}_2/\mathcal{N}_{2crit}$	$\omega_{1c}^2/\omega_{1\text{ no load}}^2$	Differences	$\omega_{1t}^2/\omega_{1\text{ no load}}^2$	Differences
0.000	0.99986338		1.00013660	
0.100	0.90020466	0.09965872	1.09975821	0.09962161
0.200	0.80037027	0.09983439	1.19948114	0.09972293
0.300	0.70049473	0.09987554	1.29917048	0.09968934
0.400	0.60057578	0.09991895	1.39882781	0.09965733
0.500	0.50061099	0.09996479	1.49845461	0.09962680
0.600	0.40059775	0.10001324	1.59805228	0.09959767
0.700	0.30053323	0.10006452	1.69762213	0.09956984
0.800	0.20041436	0.10011887	1.79716537	0.09954324
0.900	0.10023782	0.10017654	1.89668315	0.09951779
1.000	0.00000000	0.10023782	1.99617657	0.09949342

$$\frac{\omega_{1c}^2}{\omega_{1\text{ no load}}^2} = -2.596\,816\,904 \times 10^{-3}\frac{\mathcal{N}_2^2}{\mathcal{N}_{2crit}^2} - 0.997\,328\,4065\frac{\mathcal{N}_2}{\mathcal{N}_{2crit}} + 0.999\,932\,6019, \tag{71a}$$

$$\frac{\omega_{1t}^2}{\omega_{1\text{ no load}}^2} = -1.310\,482\,273 \times 10^{-3}\frac{\mathcal{N}_2^2}{\mathcal{N}_{2crit}^2} + 0.997\,432\,2238\frac{\mathcal{N}_2}{\mathcal{N}_{2crit}} + 1.000\,058\,716. \tag{71b}$$

Table 7. Computational results for $\nu = 0.9$ and $b = 0.5$

$N/N_{crit} = \mathcal{N}_2/\mathcal{N}_{2crit}$	$\omega_{1c}^2/\omega_{1\text{ no load}}^2$	Differences	$\omega_{1t}^2/\omega_{1\text{ no load}}^2$	Differences
0.000	0.99987327		1.00012673	
0.100	0.90032899	0.09954428	1.09961298	0.09948625
0.200	0.80059649	0.09973249	1.19917114	0.09955816
0.300	0.70079878	0.09979771	1.29867743	0.09950629
0.400	0.60093180	0.09986698	1.39813462	0.09945719
0.500	0.50099116	0.09994064	1.49754526	0.09941064
0.600	0.40097208	0.10001908	1.59691174	0.09936648
0.700	0.30086936	0.10010271	1.69623628	0.09932454
0.800	0.20067734	0.10019202	1.79552097	0.09928468
0.900	0.10038982	0.10028753	1.89476772	0.09924676
1.000	0.00000000	0.10038982	1.99397837	0.09921065

$$\frac{\omega_{1c}^2}{\omega_{1\text{ no load}}^2} = -4.104\,840\,441 \times 10^{-3}\frac{\mathcal{N}_2^2}{\mathcal{N}_{2crit}^2} - 0.995\,790\,1871\frac{\mathcal{N}_2}{\mathcal{N}_{2crit}} + 0.999\,920\,6831, \tag{72a}$$

$$\frac{\omega_{1t}^2}{\omega_{1\text{ no load}}^2} = -2.080\,081\,369\times 10^{-3}\frac{\mathcal{N}_2^2}{\mathcal{N}_{2crit}^2} + 0.9959923923\frac{\mathcal{N}_2}{\mathcal{N}_{2crit}} + 1.000\,062431. \tag{72b}$$

Table 8. Computational results for $\nu = 0.9$ and $b = 0.6$

$N/N_{crit} = \mathcal{N}_2/\mathcal{N}_{2crit}$	$\omega_{1c}^2/\omega_{1\text{ no load}}^2$	Differences	$\omega_{1t}^2/\omega_{1\text{ no load}}^2$	Differences
0.000	0.99988350		1.00011651	
0.100	0.90032837	0.09955513	1.09961538	0.09949887
0.200	0.80059672	0.09973165	1.19917793	0.09956255
0.300	0.70080097	0.09979575	1.29869081	0.09951288
0.400	0.60093665	0.09986431	1.39815694	0.09946613
0.500	0.50099889	0.09993777	1.49757901	0.09942207
0.600	0.40098229	0.10001659	1.59695951	0.09938050
0.700	0.30088097	0.10010132	1.69630074	0.09934123
0.800	0.20068841	0.10019256	1.79560483	0.09930409
0.900	0.10039741	0.10029100	1.89487377	0.09926894
1.000	0.00000000	0.10039741	1.99410940	0.09923563

$$\frac{\omega_{1c}^2}{\omega_{1\text{ no load}}^2} = -4.123\,396\,713\times10^{-3}\frac{\mathcal{N}_2^2}{\mathcal{N}_{2crit}^2} - 0.995\,764\,61\frac{\mathcal{N}_2}{\mathcal{N}_{2crit}} + 0.999\,919\,997\,9, \quad (73a)$$

$$\frac{\omega_{1t}^2}{\omega_{1\text{ no load}}^2} = -1.964\,394\,841\times10^{-3}\frac{\mathcal{N}_2^2}{\mathcal{N}_{2crit}^2} + 0.996\,009\,0117\frac{\mathcal{N}_2}{\mathcal{N}_{2crit}} + 1.000\,059\,584. \quad (73b)$$

Table 9. Computational results for $\nu = 0.9$ and $b = 0.8$

$N/N_{crit} = \mathcal{N}_2/\mathcal{N}_{2crit}$	$\omega_{1c}^2/\omega_{1\text{ no load}}^2$	Differences	$\omega_{1t}^2/\omega_{1\text{ no load}}^2$	Differences
0.000	0.99989764		1.00010236	
0.100	0.90003396	0.09986368	1.09996006	0.09985771
0.200	0.80006160	0.09997236	1.19991449	0.09995442
0.300	0.70008252	0.09997908	1.29986357	0.09994909
0.400	0.60009631	0.09998621	1.39980760	0.09994403
0.500	0.50010250	0.09999381	1.49974684	0.09993923
0.600	0.40010058	0.10000191	1.59968151	0.09993468
0.700	0.30009002	0.10001057	1.69961186	0.09993035
0.800	0.20007019	0.10001983	1.79953809	0.09992623
0.900	0.10004044	0.10002975	1.89946039	0.09992230
1.000	0.00000002	0.10004042	1.99937895	0.09991856

$$\frac{\omega_{1c}^2}{\omega_{1\text{ no load}}^2} = -5.252\,032\,453\times10^{-4}\frac{\mathcal{N}_2^2}{\mathcal{N}_{2crit}^2} - 0.999\,440\,542\,7\frac{\mathcal{N}_2}{\mathcal{N}_{2crit}} + 0.999\,959\,9196, \quad (74a)$$

$$\frac{\omega_{1t}^2}{\omega_{1\text{ no load}}^2} = -1.137\,211\,210\times10^{-4}\frac{\mathcal{N}_2^2}{\mathcal{N}_{2crit}^2} + 0.999\,462\,7271\frac{\mathcal{N}_2}{\mathcal{N}_{2crit}} + 1.000\,038\,224. \quad (74b)$$

8.2.2. *Solutions to Problem 2.*

Table 10. Computational results for $\nu = 0.8$ and $b = 0.2$

$N/N_{crit} = \mathcal{N}_2/\mathcal{N}_{2crit}$	$\omega_{1c}^2/\omega_{1\text{ no load}}^2$	Differences	$\omega_{1t}^2/\omega_{1\text{ no load}}^2$	Differences
0.000	0.99985219		1.00014779	
0.100	0.90004447	0.09980773	1.09994714	0.09979935
0.200	0.80008021	0.09996426	1.19988624	0.09993910
0.300	0.70010685	0.09997336	1.29981761	0.09993137
0.400	0.60012397	0.09998288	1.39974153	0.09992392
0.500	0.50013114	0.09999283	1.49965827	0.09991675
0.600	0.40012789	0.10000325	1.59956811	0.09990983
0.700	0.30011372	0.10001417	1.69947127	0.09990316
0.800	0.20008809	0.10002564	1.79936799	0.09989672
0.900	0.10005039	0.10003770	1.89925848	0.09989049
1.000	0.00000000	0.10005039	1.99914295	0.09988447

$$\frac{\omega_{1c}^2}{\omega_{1\text{ no load}}^2} = -6.912\,436\,031 \times 10^{-4}\frac{\mathcal{N}_2^2}{\mathcal{N}_{2crit}^2} - 0.999\,263\,3476\frac{\mathcal{N}_2}{\mathcal{N}_{2crit}} + 0.999\,943\,9839, \tag{75a}$$

$$\frac{\omega_{1t}^2}{\omega_{1\text{ no load}}^2} = -1.802\,051\,770 \times 10^{-4}\frac{\mathcal{N}_2^2}{\mathcal{N}_{2crit}^2} + 0.999\,281\,1886\frac{\mathcal{N}_2}{\mathcal{N}_{2crit}} + 1.000\,054\,509. \tag{75b}$$

Table 11. Computational results for $\nu = 0.8$ and $b = 0.4$

$N/N_{crit} = \mathcal{N}_2/\mathcal{N}_{2crit}$	$\omega_{1c}^2/\omega_{1\text{ no load}}^2$	Differences	$\omega_{1t}^2/\omega_{1\text{ no load}}^2$	Differences
0.000	0.99987346		1.00012652	
0.100	0.90062605	0.09924741	1.09925682	0.09913030
0.200	0.80112977	0.09949628	1.19840145	0.09914463
0.300	0.70150559	0.09962418	1.29743850	0.09903705
0.400	0.60174757	0.09975802	1.39637232	0.09893382
0.500	0.50184936	0.09989821	1.49520701	0.09883468
0.600	0.40180417	0.10004519	1.59394643	0.09873942
0.700	0.30160473	0.10019944	1.69259424	0.09864781
0.800	0.20124325	0.10036148	1.79115389	0.09855966
0.900	0.10071134	0.10053191	1.88962866	0.09847477
1.000	0.00000000	0.10071134	1.98802165	0.09839298

$$\frac{\omega_{1c}^2}{\omega_{1\text{ no load}}^2} = -7.537\,051\,383 \times 10^{-3}\frac{\mathcal{N}_2^2}{\mathcal{N}_{2crit}^2} - 0.992\,328\,968\,6\frac{\mathcal{N}_2}{\mathcal{N}_{2crit}} + 0.999\,906\,4673, \tag{76a}$$

$$\frac{\omega_{1t}^2}{\omega_{1\text{ no load}}^2} = -4.640\,413\,266 \times 10^{-3}\frac{\mathcal{N}_2^2}{\mathcal{N}_{2crit}^2} + 0.992\,575\,2561\frac{\mathcal{N}_2}{\mathcal{N}_{2crit}} + 1.000\,072\,981. \tag{76b}$$

Table 12. Computational results for $\nu = 0.8$ and $b = 0.5$

$N/N_{crit} = \mathcal{N}_2/\mathcal{N}_{2crit}$	$\omega_{1c}^2/\omega_{1\text{ no load}}^2$	Differences	$\omega_{1t}^2/\omega_{1\text{ no load}}^2$	Differences
0.000	0.99988983		1.00011019	
0.100	0.90114665	0.09874319	1.09864583	0.09853564
0.200	0.80207470	0.09907195	1.19709441	0.09844858
0.300	0.70277232	0.09930238	1.29535536	0.09826095
0.400	0.60322679	0.09954553	1.39343768	0.09808232
0.500	0.50342440	0.09980239	1.49134978	0.09791211
0.600	0.40335040	0.10007400	1.58909957	0.09774979
0.700	0.30298888	0.10036152	1.68669445	0.09759488
0.800	0.20232264	0.10066624	1.78414136	0.09744691
0.900	0.10133306	0.10098957	1.88144685	0.09730549
1.000	0.00000000	0.10133306	1.97861707	0.09717021

$$\frac{\omega_{1c}^2}{\omega_{1\text{ no load}}^2} = -1.381\,407\,376 \times 10^{-2}\frac{\mathcal{N}_2^2}{\mathcal{N}_{2crit}^2} - 0.985\,936\,3720\frac{\mathcal{N}_2}{\mathcal{N}_{2crit}} + 0.999\,855\,375\,9, \tag{77a}$$

$$\frac{\omega_{1t}^2}{\omega_{1\text{ no load}}^2} = -8.037\,238\,551 \times 10^{-3}\frac{\mathcal{N}_2^2}{\mathcal{N}_{2crit}^2} + 0.986\,515\,837\,5\frac{\mathcal{N}_2}{\mathcal{N}_{2crit}} + 1.000\,096\,317. \tag{77b}$$

Table 13. Computational results for $\nu = 0.8$ and $b = 0.6$

$N/N_{crit} = \mathcal{N}_2/\mathcal{N}_{2crit}$	$\omega_{1c}^2/\omega_{1\text{ no load}}^2$	Differences	$\omega_{1t}^2/\omega_{1\text{ no load}}^2$	Differences
0.000	0.99990727		1.00009273	
0.100	0.90148845	0.09841882	1.09825700	0.09816427
0.200	0.80270523	0.09878321	1.19627516	0.09801816
0.300	0.70363169	0.09907354	1.29406894	0.09779378
0.400	0.60424744	0.09938425	1.39165166	0.09758272
0.500	0.50453016	0.09971728	1.48903562	0.09738396
0.600	0.40445537	0.10007479	1.58623218	0.09719656
0.700	0.30399619	0.10045919	1.68325185	0.09701967
0.800	0.20312300	0.10087319	1.78010438	0.09685253
0.900	0.10180313	0.10131987	1.87679882	0.09669444
1.000	0.00000046	0.10180267	1.97334357	0.09654475

$$\frac{\omega_{1c}^2}{\omega_{1\text{ no load}}^2} = -1.820\,778\,680 \times 10^{-2}\frac{\mathcal{N}_2^2}{\mathcal{N}_{2crit}^2} - 0.981\,395\,528\,8\frac{\mathcal{N}_2}{\mathcal{N}_{2crit}} + 0.999\,791\,5525, \tag{78a}$$

$$\frac{\omega_{1t}^2}{\omega_{1\text{ no load}}^2} = -9.\,344\,847\,633 \times 10^{-3}\frac{\mathcal{N}_2^2}{\mathcal{N}_{2crit}^2} + 0.982\,506\,6770\frac{\mathcal{N}_2}{\mathcal{N}_{2crit}} + 1.000\,115\,576. \tag{78b}$$

Table 14. Computational results for $\nu = 0.8$ and $b = 0.8$

$N/N_{crit} = \mathcal{N}_2/\mathcal{N}_{2crit}$	$\omega^2_{1c}/\omega^2_{1\text{ no load}}$	Differences	$\omega^2_{1t}/\omega^2_{1\text{ no load}}$	Differences
0.000	0.99993292		1.00006707	
0.100	0.90028412	0.09964880	1.09966903	0.09960196
0.200	0.80051788	0.09976624	1.19929442	0.09962540
0.300	0.70069738	0.09982051	1.29887909	0.09958467
0.400	0.60081828	0.09987910	1.39842568	0.09954659
0.500	0.50087577	0.09994251	1.49793660	0.09951093
0.600	0.40086450	0.10001127	1.59741409	0.09947748
0.700	0.30077846	0.10008604	1.69686015	0.09944607
0.800	0.20061092	0.10016754	1.79627667	0.09941652
0.900	0.10035429	0.10025663	1.89566536	0.09938869
1.000	0.00000000	0.10035429	1.99502779	0.09936244

$$\frac{\omega^2_{1c}}{\omega^2_{1\text{ no load}}} = -3.574\,398\,585 \times 10^{-3}\frac{\mathcal{N}_2^2}{\mathcal{N}_{2crit}^2} - 0.996\,325\,2147\frac{\mathcal{N}_2}{\mathcal{N}_{2crit}} + 0.999\,937\,4502, \tag{79a}$$

$$\frac{\omega^2_{1t}}{\omega^2_{1\text{ no load}}} = -1.613\,827\,513 \times 10^{-3}\frac{\mathcal{N}_2^2}{\mathcal{N}_{2crit}^2} + 0.996\,593\,5135\frac{\mathcal{N}_2}{\mathcal{N}_{2crit}} + 1.000\,040\,048. \tag{79b}$$

Remark 15. The differences listed in the tables vary very little as a function of N/N_{crit}: they can be considered practically constant. It is also worth noting that the largest change in value (which is still a very small change in value) concerning the differences is for the value $b = 0.5$, where the change in cross section is at the central point of the beam.

9. Concluding remarks

Making use of the definition presented in [18] for the Green functions of coupled boundary value problems, the paper has presented the Green functions of pinned-pinned stepped beams with heterogeneous cross section provided that (a) no axial load is exerted on the beam, (b) the beam is subjected to a compressive axial force, and (c) a tensile axial force is exerted on the beam. The eigenvalue problem related to the free vibrations of the pinned-pinned stepped beams is reduced to an eigenvalue problem governed by a homogeneous Fredholm integral equation. The vibration problems of the axially loaded stepped beams are also reduced to two Fredholm integral equations. Then these eigenvalue problems are solved numerically and the computational results are presented. It is a well known result that the equations

$$\frac{\omega^2_{1c}}{\omega^2_{1\text{ no load}}} = 1.0 - \frac{\mathcal{N}}{\mathcal{N}_{crit}}, \qquad \frac{\omega^2_{1t}}{\omega^2_{1\text{ no load}}} = 1.0 + \frac{\mathcal{N}}{\mathcal{N}_{crit}} \tag{80}$$

are the solutions to a similar problem for simply supported homogeneous and heterogeneous beams – in the second case cross sectional heterogeneity is assumed. According to our computational results, equations (80) provide very good solutions for both pinned-pinned and stepped beams – the maximum of the relative error in $\omega^2_{1t}/\omega^2_{1\text{ no load}}$ for $\nu = 0.8$, $b = 0.5$ and $\mathcal{N}/\mathcal{N}_{crit} = 1.0$ is 1.069% (see Table 12).

Appendix A. Stability problem of pinned-pinned stepped beams

The stability problem of stepped beams is governed by ODEs (51) associated with boundary and continuity conditions (27). Making use of the solutions given by equations (54), the eigenvalue problem (51), (27) with $p_2 = \sqrt{\mathcal{N}_2}$ as the eigenvalue yields the following homogeneous equation system for the unknown integration constants:

$$\begin{bmatrix} 1 & 0 & 1 & 0 & 0 & 0 & 0 & 0 \\ 0 & 0 & 1 & 0 & 0 & 0 & 0 & 0 \\ 1 & b & \cos bp_2\gamma & \sin bp_2\gamma & -1 & -b & -\cos p_2 b & -\sin p_2 b \\ 0 & 1 & -p_2\gamma\sin bp_2\gamma & p_2\gamma\cos bp_2\gamma & 0 & -1 & p_2\sin p_2 b & -p_2\cos p_2 b \\ 0 & 0 & -\cos bp_2\gamma & -\sin bp_2\gamma & 0 & 0 & \cos p_2 b & \sin p_2 b \\ 0 & 0 & \gamma\sin bp_2\gamma & -\gamma\cos bp_2\gamma & 0 & 0 & -\sin p_2 b & \cos p_2 b \\ 0 & 0 & 0 & 0 & 1 & \ell & \cos p_2\ell & \sin p_2\ell \\ 0 & 0 & 0 & 0 & 0 & 0 & \cos p_2\ell & \sin p_2\ell \end{bmatrix} \begin{bmatrix} a_{11} \\ a_{21} \\ a_{31} \\ a_{41} \\ a_{12} \\ a_{22} \\ a_{32} \\ a_{42} \end{bmatrix} = \begin{bmatrix} 0 \\ 0 \\ 0 \\ 0 \\ 0 \\ 0 \\ 0 \\ 0 \end{bmatrix} \tag{81}$$

$$\gamma = \sqrt{\alpha}$$

The characteristic equation is the determinant of the coefficient matrix

$$\mathcal{D} = -\gamma\ell\cos b\gamma p_2 \sin p_2(\ell - b) - \ell\sin b\gamma p_2\cos p_2(\ell - b) = 0. \tag{82}$$

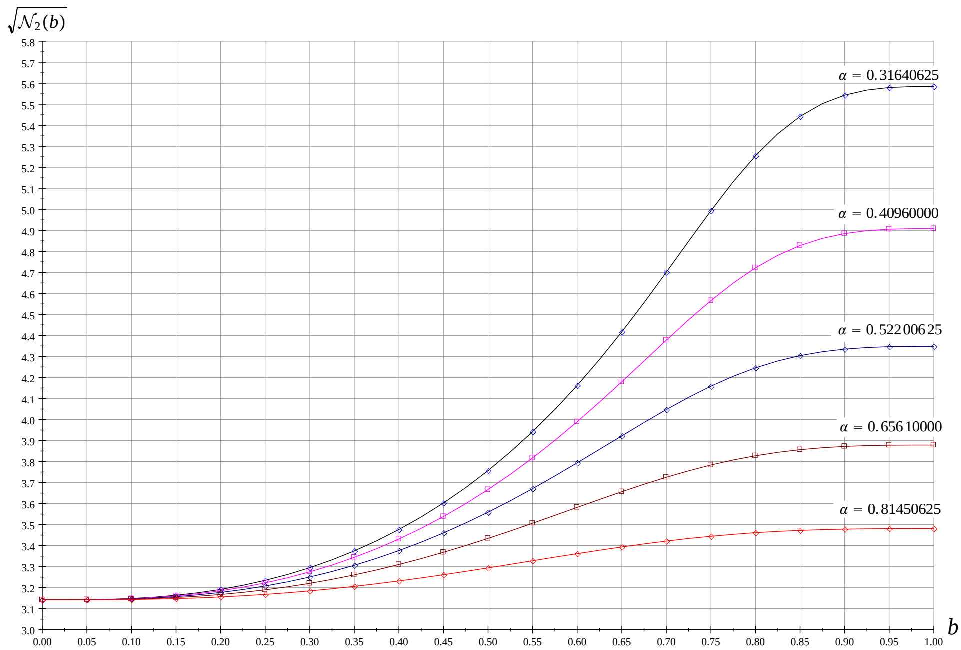

Figure 8. Critical force against b, α is a parameter

Remark 16. Assume that $\alpha = b = \ell = 1$ and $p_2 = p$. Then we get the characteristic equation for a uniform fixed-fixed beam

$$\mathcal{D} = \sin p = 0 \tag{83}$$

where $p = \pi$ is the smallest root for p.

Equation (82) has been solved numerically. Figure 8 shows the critical force $\sqrt{N_{2\,\mathrm{crit}}(b)}$ against b obtained from the numerical solution mentioned.

References

1. Cannizzaro, F., Fiore, I., Caddemi, S., and Caliò, I. "The exact distributional model for free vibrations of shear-bending multi-cracked Timoshenko beams." *European Journal of Mechanics - A/Solids,* **101**, (2023), p. 105039. doi: 10.1016/j.euromechsol.2023.105039.
2. Su, J., Zhang, K., and Zhang, Q. "Vibration analysis of coupled straight curved beam systems with arbitrary discontinuities subjected to various harmonic forces." *Archive of Applied Mechanics,* **90**, (2020), pp. 2071–2090. doi: 10.1007/s00419-020-01709-z.
3. Shun-Cai, Li, Li, Liang, and Qiu, Yu. "Natural frequency of bending vibration for stepped beam of different geometrical characters and materials." *Noise & Vibration Worldwide,* **50**(1), (2019), pp. 3–12. doi: 10.1177/0957456518812800.
4. Mirzabeigy, A. and Madoliat, R. "Large amplitude free vibration of axially loaded beams resting on variable elastic foundation." *Alexandria Engineering Journal,* **55**(2), (2016), pp. 1107–1114. doi: 10.1016/j.aej.2016.03.021.
5. Stojanovic, V., Kozic, P., Pavlovic, R., and Janevski, G. "Effect of rotary inertia and shear on vibration and buckling of a double beam system under compressive axial loading." *Archive of Applied Mechanics,* **81**, (2011), pp. 1993–2005. doi: 10.1007/s00419-011-0532-1.
6. Barari, A., Kaliji, H. D., Ghadimi, M., and Domiarry, G. "Non-linear vibration of Euler-Bernoulli beams." *Latin American Journal of Solids and Structures,* **8**, (2011), pp. 139–148. doi: 10.1590/S1679-78252011000200002.
7. Jong-Shyong Wu and Bo-Hau Chang. "Free vibration of axial-loaded multi-step Timoshenko beam carrying arbitrary concentrated elements using continuous-mass transfer matrix method." *European Journal of Mechanics - A/Solids,* **38**, (2013), pp. 20–37. doi: 10.1016/j.euromechsol.2012.08.003.
8. De Rosa, M. A., Bellés, P. M., and Maurizi, M. J. "Free vibrations of stepped beams with intermediate elastic supports." *Journal of Sound and Vibration,* **181**(5), (1995), pp. 905–910. doi: 10.1006/jsvi.1995.0177.
9. Mahmoud, M. A. "Free vibrations of tapered and stepped, axially functionally graded beams with any number of attached masses." *Engineering Structures,* **267**, (2022), p. 114696. doi: 10.1016/j.engstruct.2022.114696.
10. Qibo, Mao. "Free vibration analysis of multiple-stepped beams by using Adomian decomposition method." *Mathematical and Computer Modelling,* **54**(1), (2011), pp. 756–764. doi: 10.1016/j.mcm.2011.03.019.

11. Green, G. *An Essay on the Application of Mathematical Analysis to the Theories of Electricity and Magnetism.* Notthingam, T. Wheelhouse, 1828.
12. Behnam-Rasouli, M. S., Challamel, N., Karamodin, A., and Aftabi Sani, A. "Application of the Green's function method for static analysis of nonlocal stress-driven and strain gradient elastic nanobeams." *International Journal of Solids and Structures* **295**, (2024), p. 112794. doi: 10.1016/j.ijsolstr.2024.112794.
13. Li, X. Z., Zhao, X., and Li, Y. H. "Green's functions of the forced vibration of Timoshenko beams with damping effect." *Journal of Sound and Vibration,* **333**(6), (2014). doi: 10.1016/j.jsv.2013.11.007.
14. Murty, S. N. and Suresh Kumar, G. "Three point boundary value problems for third order fuzzy differential equations." *Journal of the Chungcheong Mathematical Sociaty,* **19**(3), (2006), pp. 101–110. doi: 10.14403/jcms.2006.19.1.101.
15. Obádovics, J. G. "On the boundary and initial value problems of differental equation systems." (in Hungarian). PhD thesis. Hungarian Academy of Sciences, 1967.
16. Szeidl, G. "Effect of the change in length on the natural frequencies and stability of circular beams." (in Hungarian). PhD thesis. Department of Mechanics, University of Miskolc, Hungary, 1975.
17. Szeidl, G. and Kiss, L. P. *Mechanical Vibrations, an Introduction.* Ed. by Vladimir I. Babitsky and Jens Wittenburg. Foundation of Engineering Mechanics. Springer Nature, Switzerland, 2020. doi: 10.1007/978-3-030-45074-8.
18. Mesaoudi, A., Kiss, L. P., and Szeidl, G. "Green functions for coupled boundary value problems with applications to stepped beams." Unpublished manuscript, available from the authors in pdf format. 2024.
19. Baksa, A. and Ecsedi, I. "A note on the pure bending of nonhomogeneous prismatic bars." *International Journal of Mechanical Engineering Education* **37**(2), (2009), pp. 1108–129. doi: 10.7227/IJMEE.37..

Notes for Contributors
to the Journal of Computational and Applied Mechanics

Aims and scope. The aim of the journal is to publish research papers on theoretical and applied mechanics. Special emphasis is given to articles on computational mechanics, continuum mechanics (mechanics of solid bodies, fluid mechanics, heat and mass transfer) and dynamics. Review papers on a research field and materials effective for teaching can also be accepted and are published as review papers or classroom notes. Papers devoted to mathematical problems relevant to mechanics will also be considered.
Frequency of the journal. Two issues a year (approximately 80 pages per issue).

Submission of Manuscripts. Submission of a manuscript implies that the paper has not been published, nor is being considered for publication elsewhere. Papers should be written in standard grammatical English. The manuscript is to be submitted in electronic, preferably in pdf, format. The text is to be 130 mm wide and 190 mm long and the main text should be typeset in 10pt CMR fonts. Though the length of a paper is not prescribed, authors are encouraged to write concisely. However, short communications or discussions on papers published in the journal must not be longer than 2 pages. Each manuscript should be provided with an English Abstract of about 50–70 words, reporting concisely on the objective and results of the paper. The Abstract is followed by the Mathematical Subject Classification – in case the author (or authors) give the classification codes – then the keywords (no more than five). References should be grouped at the end of the paper in numerical order of appearance. Author's name(s) and initials, paper titles, journal name, volume, issue, year and page numbers should be given for all journals referenced.
The journal prefers the submission of manuscripts in LaTeX. Authors should select the AMS-LaTeX article class and are not recommended to define their own LaTeX commands. Visit our home page for further details concerning how to edit your paper.
Manuscripts should be sent to either to the Editorial Office of JCAM:

jcam@uni-miskolc.hu

or directly to the editor-in-chief: Balázs Tóth

balazs.toth@uni-miskolc.hu

The eventual supply of an accepted for publication paper in its final camera-ready form will ensure more rapid publication. Format requirements are provided by the home page of the journal from which sample LaTeX files can be downloaded:

`http://www.mech.uni-miskolc.hu/jcam/`

These sample files can also be obtained directly (via e-mail) from Balázs Tóth.

One issue of the journal will be provided free of charge and mailed to the correspondent author. Since JCAM is an open access journal each paper can be downloaded freely from the homepage of the journal.

The Journal of Computational and Applied Mechanics is abstracted in Zentralblatt für Mathematik and in the Russian Referativnij Zhurnal.

Secretariat of the Vice-Rector for Research and International Relations, University of Miskolc
Responsible for publication: Prof. dr. Zita Horváth, rector
Published by the Miskolc University Press under the leadership of Attila Szendi
Responsible for duplication: Works manager Erzsébet Pásztor
Number of copies printed: 75
Put to the Press on February 18, 2025
Number of permission: TNI.2025-40.ME.

ISSN 2732–0189 (Online)
ISSN 1586–2070 (Print)

A Short History of the Publications of the University of Miskolc

The University of Miskolc (Hungary) is an important center of research in Central Europe. Its parent university was founded by the Empress Maria Teresia in Selmecbánya (today Banska Štiavnica, Slovakia) in 1735. After the first World War the legal predecessor of the University of Miskolc moved to Sopron (Hungary) where, in 1929, it started the series of university publications with the title *Publications of the Mining and Metallurgical Division of the Hungarian Academy of Mining and Forestry Engineering* (Volumes I.–VI.). From 1934 to 1947 the Institution had the name Faculty of Mining, Metallurgical and Forestry Engineering of the József Nádor University of Technology and Economic Sciences at Sopron. Accordingly, the publications were given the title *Publications of the Mining and Metallurgical Engineering Division* (Volumes VII.–XVI.). For the last volume before 1950 – due to a further change in the name of the Institution – *Technical University, Faculties of Mining, Metallurgical and Forestry Engineering, Publications of the Mining and Metallurgical Divisions* was the title.
For some years after 1950 the Publications were temporarily suspended.
After the foundation of the Mechanical Engineering Faculty in Miskolc in 1949 and the movement of the Sopron Mining and Metallurgical Faculties to Miskolc, the Publications restarted with the general title *Publications of the Technical University of Heavy Industry* in 1955. Four new series – Series A (Mining), Series B (Metallurgy), Series C (Machinery) and Series D (Natural Sciences) – were founded in 1976. These came out both in foreign languages (English, German and Russian) and in Hungarian.
In 1990, right after the foundation of some new faculties, the university was renamed to University of Miskolc. At the same time the structure of the Publications was reorganized so that it could follow the faculty structure. Accordingly three new series were established: Series E (Legal Sciences), Series F (Economic Sciences) and Series G (Humanities and Social Sciences). The latest series, i.e., the series H (European Integration Studies) was founded in 2001. The eight series are formed by some periodicals and such publications which come out with various frequencies.
Papers on computational and applied mechanics were published in the

Publications of the University of Miskolc, Series D, Natural Sciences.

This series was given the name Natural Sciences, Mathematics in 1995. The name change reflects the fact that most of the papers published in the journal are of mathematical nature though papers on mechanics also come out.
The series

Publications of the University of Miskolc, Series C, Fundamental Engineering Sciences

founded in 1995 also published papers on mechanical issues. The present journal, which is published with the support of the Faculty of Mechanical Engineering and Informatics as a member of the Series C (Machinery), is the legal successor of the above journal.

Journal of Computational and Applied Mechanics
Volume 19, Number 2 (2024)

Contents

Contributed Papers